VOLUMETRIC HEAT TRANSFER VIA CONSTRUCTAL THEORY, AND ITS

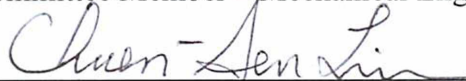APPLICATIONS IN PERMAFROST AND HYDROGEN ENERGY STORAGE

By

Vamsi Krishna Kukkapalli

RECOMMENDED:

Dr. Debendra Das
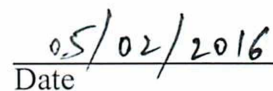Committee Member – Mechanical Engineering

Dr. Chuen-Sen Lin
Committee Member – Mechanical Engineering

Dr. Sun Woo Kim
Advisory Committee Chair – Mechanical Engineering

Dr. Rorik A. Peterson
Chair, Department of Mechanical Engineering

05/02/2016
Date

VOLUMETRIC HEAT TRANSFER VIA CONSTRUCTAL THEORY, AND ITS

APPLICATIONS IN PERMAFROST AND HYDROGEN ENERGY STORAGE

A

PROJECT

Presented to the Faculty

of the University of Alaska Fairbanks

in Partial Fulfillment of the Requirements

for the Degree of

MASTER OF SCIENCE

By

Vamsi Krishna Kukkapalli, B.S.

Fairbanks, AK

May 2016

Abstract

Constructal theory is widely used as a powerful tool in designing of engineering systems (flow configurations, patterns, geometry). This theory is observed in nature and its principles are applicable to general engineering. Constructal theory encompasses a wide range of space in the "design", drawing from each and every field from engineering to biology. The universal design of nature and the constructal law unify all animate schemata such as human blood circulatory systems, and inanimate systems, such as urban traffic and river basins. The proceeding research applies the overlying theories of constructal theory to the two different systems in order to achieve best thermal performance phenomena.

The first is stabilization of roadway embankments in the permafrost regions with design modifications in existing thermosyphon evaporators with tree structure designs, and defining the optimal spacing between two neighboring thermosyphons based on thermal cooling phenomena. This research utilizes constructal law to the generation of tree-shaped layouts for fluid flow, so that the flow structures use the available space in optimally. The intention here is the optimization of geometry of the flow system. This begins with the most simple cases of tree-shaped flows: T- and Y-shaped constructs, the purpose of which is to create a flow connection between one point (defined as a "source" or "sink") to an infinity of points (via a line/area/volume). Empirically speaking, tree-shaped flows are natural examples of self-organization and optimization. By contrast, constructal law is theory which states that flow architectures such as these are the evolutionary results of nature which tend toward greater global flow access. Tree-shaped flows can be derived from this constructal law. The mathematical simulation revealed that there exists an optimal spacing between two neighboring

thermosyphons, and the tree structures perform better than the existing configuration in terms of thermal cooling.

The second part of the research is to find an effective way to reject heat released from the metal hydride powder to the outer environment during the hydrogen absorption process. The main objective of this investigation is to minimize the time required for the absorption process, and to reduce the hotspot temperature by determining the optimal aspect ratio of rectangular fins, while the total volume of fins used is kept constant. The intension of using constructal theory in this part of research is to find the optimal geometrical parameters (length, width) of the fin structure for better thermal performance of the metal hydride reactor system. The simulations revealed that there exists an optimum aspect ratio of rectangular fins for accelerating heat rejection and lowering the hotspot temperature in a cylindrical metal hydride reactor.

Constructal theory is supremely adapted for use in 2-dimensional and 3-dimensional design for heat transfer structures, as it allows for incorporation of minute analysis of the interior structure with the goal of optimizing for heat transfer. In its application in the realm of engineering, every multidimensional solid structure that is to be cooled, heated or serviced by fluid streams must be vascularized. By this definition, 'vascularization' includes, however is not limited to, structures such as trees, geometrical spacing, and solid walls. Here, every geometric detail will be sized and positioned to achieve maximum efficacy from an engineering design point of view. Furthermore, via design morphing we can achieve low resistances in flow structures which are applicable in cooling and heating applications. An example is that of a ground-source heat pump design where the piping design is morphed by constructal law and spaced in an optimal way to achieve maximum thermal efficiency when extracting heat from the ground.

Table of Contents

List of Figures

List of Tables

Chapter 1 Introduction

1.1   Constructal law in evolution of design

The design flow nature is goverened by the constructal law which is first formulated by Adian Bejan in 1996, which gives a gerneral explanation on why we see recurring configurations on every scale. It is stated as " For a finite size flow system to persist in time (to live), its configuration must evolve in such a way that provide easier access to the currents that flow through it [1]."

In each and every aspect in a nature we see the different design configurations. Why do simulations of the dark matter in universe, shape of the lightning bolt, shape of the galaxies, human blood circulatory system, brain nueral system, and the shape of the lightning all look alike? The fundamental idea of the constuctal law is: every system has a flow configuration, whether it is animate or inanimate has to be undergone some resistance in order to flow. However, according to Bejan, the flow systems in the nature has evolved in way that they provide the greater access to flow in time. Figures 1.1 & 1.2

For example, we see the numerous examples of the constructal law in respect to animate and inanimate systems. It consits of two basic properties current that is flowing (mass, fluid, transport, heat etc.)and the shape configurations through wich the current flows. For a case river basin's evolve in such a way that it transports water (current) from an area to the river mouth. Same way, lightning bolt it produces enormous amount of the electricity (current) which is developed in an optimized branched structure to transport from the clouds to another cloud or a point in an efficient way and quick time. While we consider the animate systems, the human blood circulatory system, where blood (current) flows through blood vessels from a point to volume.

The current research constructal theory is used to develop optimal heat transfer structure for two different applications. The first is in the thermosyphon evaporator which is used to stabilize the roadway embankments in the permafrost zone. The thermosyphon evaporator which is burried under the roadway, is the fundamental pathway to extract heat from the underground. The thermosyphon principle is transferring working fluid from point to point

1

flow, which is the basic concept of the constructal design for any flow system. By utilizing constructal design, the evaporator is morphed in a way, that it can provide greater and greater access to its currents (heat transfer) flowing through it. The second part of the research is metal hydride for hydogen energy storage, metal hydrides are one of the promising technologies for hydrogen energy storage in point of safety. The hydrogen absorption process is exothermic reaction, where heat is generated in the metal hydride rector, uneven heat distribution may leads in damaging the interior part of reactor. The constructal theory is used in deriving optimal aspect ratio of the rectangular fin structure, which can distribute efficient way to reject heat from metal hydride reactor to outside environment and moreover, it leads in accelerating hydrogen absorption process.
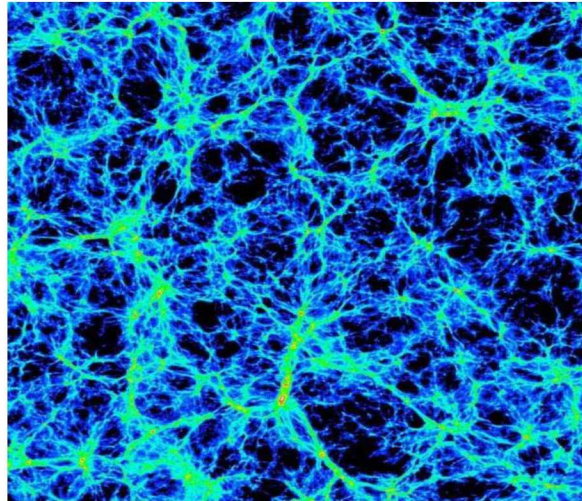
Figure: 1.1: Evidence of constructal law dark matter simulation [2]

Figure: 1.2: Evidence of constructal law lightning bolt [3]

1.2   Application 1: Permafrost

Permafrost was first defined by S.W. Muller in 1947 as a thickness of soil, sediment, or bedrock (applies to all lithospheric material) at variable depth beneath the surface experiencing a temperature continuously below freezing (0°C) for a prolonged period (Muller considered it as more than two consecutive years) [4].
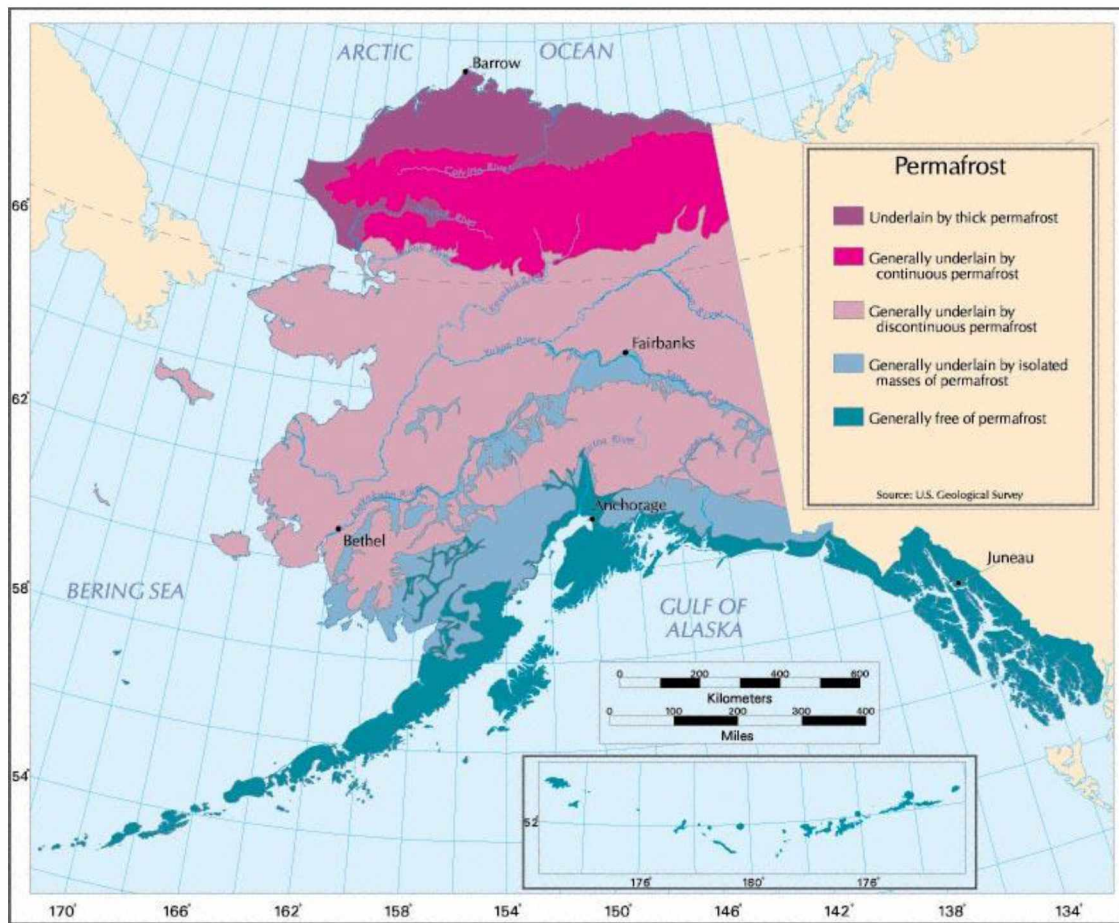
Figure: 1.3: Permafrost distribution over Alaska [5]

1.2.1 Engineering structures in permafrost zone

Permafrost soil tends to thaw due to the shifting thermal regime. Stabilizing the thaw-settlements under the engineering structures in the permafrost zones is a highly technical engineering challenge. Buildings, construction of dams, roadway, and railway embankments etc. will fall under this category. Roadway embankments are one of various engineering structures that contribute to failure due to thawing permafrost. Roadway embankments constructed in the permafrost zones have shifting thermal regime since they modify ground surface energy balance. Due to this shifting thermal regime, permafrost thaws with respect to seasonal variations, this contributes to loss of potency in foundation soil. This causes failure and instability of embankment results in outward movement of bottom side embankment. The

4

ground surface energy balance of the embankment mainly depends on numerous factors such as radiation, atmospheric air temperature, flora, etc. These factors influence the mean average surface temperature (MAST), and therefore it can differ from the mean average air temperature (MAAT). Due to this difference variation in thermal regime occurring in the ground, this often times results in thawing permafrost under roadway embankments.

Figure: 1.4: Waviness in roadway embankment due to thawing permafrost

1.2.2 Solutions for Stabilizing Roadway embankments in permafrost zone

Engineers will overcome several challenges while constructing the roadways over embankments, but embankment deformation is the one of the dangerous problem. The main reason for this type is the disturbance of the native soil while constructing the surface facilities. Native soil remains undisturbed for several hundreds of years before they begin the constructions on it and it will reach its own thermal equilibrium state. Construction activities, such as removal of vegetation and topsoil, grubbing will disturb the thermal equilibrium state of

5

the ground and removal of vegetation influences the solar absorption and precipitation. These factors will greatly affect the previously frozen ground often begin to thawing and consolidation. There are varieties of solutions available to stabilize embankment soils. According to the thermal performance they are placed in the descending order from "active cooling" to "passive cooling". Active cooling is the best method, which removes greater amount of heat from the embankment and passive cooling is one which shows less performance than active cooling methods in removing heat from ground.

Active Cooling
- Thermosyphons

- Cooling Pipes
- Ventiduct Embankment

- Crushed stone Embankments
- Block Stone Embankments

- Snow Sheds
- Shading Boards/ Awnings

Passive cooling
- Insulation (foam board, wood chips, peat, etc.)
- Embankment Widening/ Berms
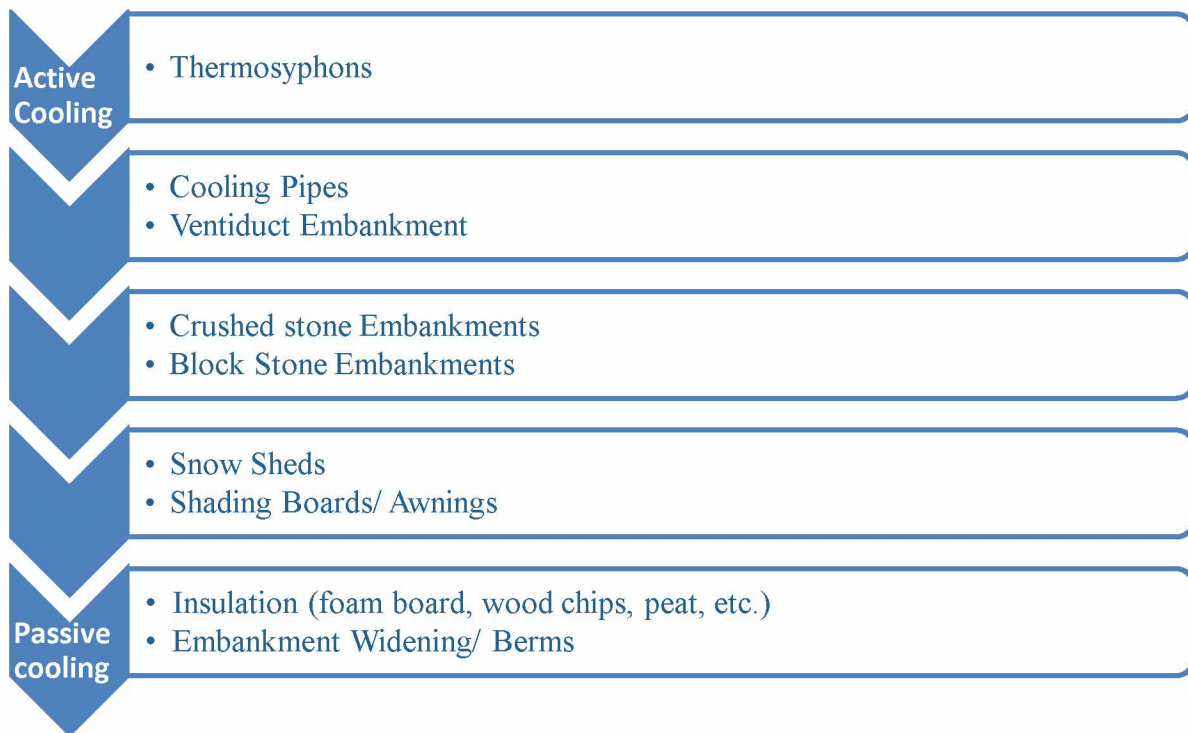
Figure: 1.5: Engineering solutions for thawing permafrost [6]

6

Table 1.2: Potential drawbacks and outcomes of different engineered solutions in permafrost [6]

Engineered solution	Expected Outcome	Potential Drawbacks	Cost ($/100 track feet)
Thermosyphons	High risk sites, unstable permafrost	Damage during transport or installation	$27,500 - $30,800
Ventiducts	Reduce internal temperature of embankments	Blockage due to snow debris, minimized performance due to settlements	$9,800- PVC $16,500- Concrete $23,750- Metal
Block Stone Embankments	Increase convection cooling and stability of embankment	Plugging due to snow	$44,800
Crushed Rock Revetments	Improve convection cooling and stability of shoulder section	Warming in center of embankment with cooling of shoulders (differential settlement) and plugging due to snow	$12,000
Awning/ Shading Board	Reduce solar radiation, improve convection cooling	Damage due to natural or manmade occurrences	------------
Extruded Polystyrene	Minimize heat influx in to soil and minimize construction depth	Water absorption, mechanical damage, decreasing insulation performance	$2300

1.2.3 Two phase closed thermosyphon

Thermosyphon is a passive heat transfer device, which is used to keep the soil in the frozen state in order to prevent thawing of the permafrost. Basically, thermosyphon is a pressurized sealed tube which is filled with low boiling point working fluids such as ammonia, carbon dioxide, Freon. It uses gravity for working fluid circulation.
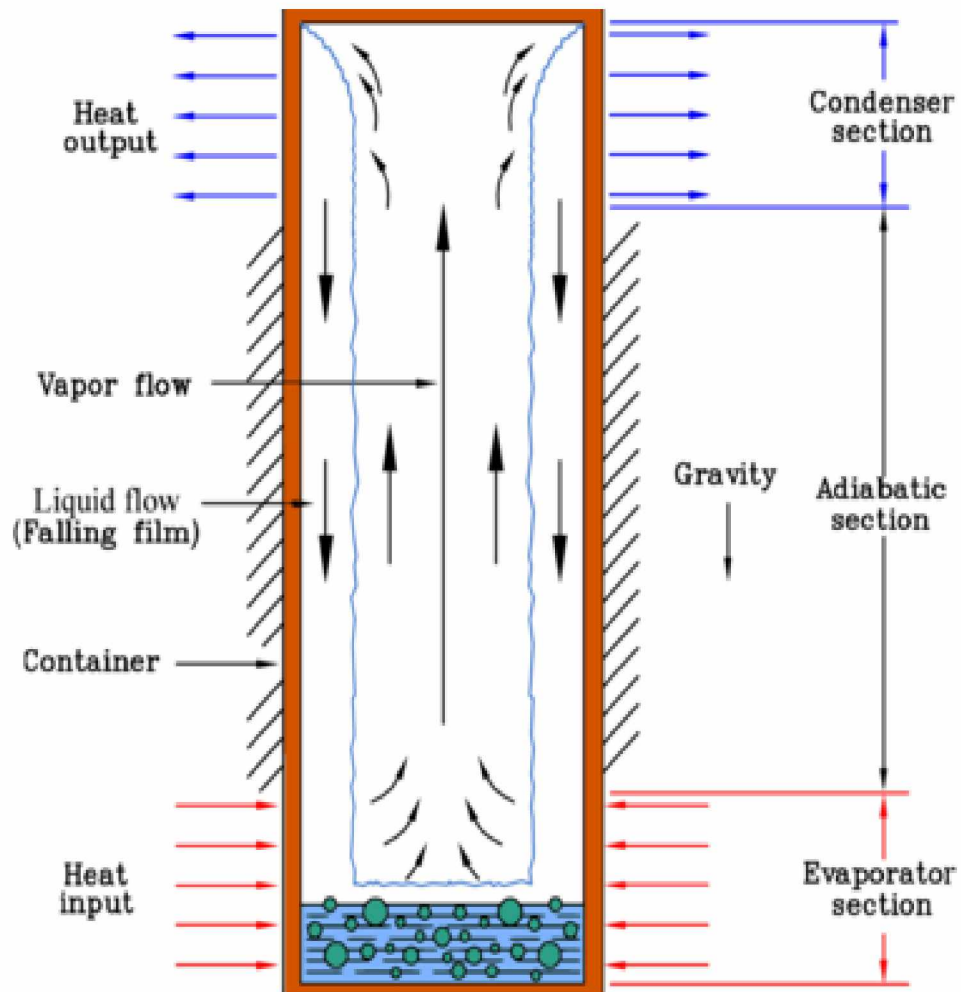
Figure: 1.6: Two phase thermosyphon [7]

Figure 1.6 represents two phase thermosyphon is a simple closed tube with low boiling point working fluid circulating inside the sealed tube. Generally, thermosyphon tube is made of high thermal conductivity and high strength metals. Thermosyphon evaporator part is buried under ground and until unless it gets heated the thermosyphon is in inactive state. Working fluid is settled at the bottom of the tube at this state. When the temperature difference occurs between the condenser and evaporator sections, heat gets absorbed from the environment boils some part of liquid settled in evaporator section. Then the vapor moves from the evaporator section to the condenser section where, the phase change heat transfer occurs between vapor and environment, causing the vapor to cool down and condensate on the condenser wall. And the phase change liquid slowly settles down to the evaporator section by gravity. This cycle repeats continuously until the thermal equilibrium is maintained between the condenser and evaporator sections. Thermosyphon applications are extended in various fields due to their outstanding heat transfer performance, including electronic cooling, nuclear reactors, arctic engineering, aerospace and automotive applications. It was first introduced in Alaska in 1960 in constructing the Trans-Alaska pipe line over 120,000 thermosyphons were used to stabilize the ground permafrost.

1.2.4   Thermosyphon designs

Thermopile: It is used to support the structures on the piles within the frozen ground layer. These are used to

•   Maintain colder temperatures, which allows to greater load bearing capacity or the increased safety factor of the pile.

•   Prevent the frost heaving of small loaded structures

•   Increase the shear and compressive strength of the frozen soil and stabilize the thawing permafrost.

Thermoprobe: It is used to keep the ground frozen around the piles or to maintain the ground frozen around the structures.

Sloped thermosyphon: In this the thermosyphon is the evaporator tubes are maintained at the slope (appx. 1:10 slope) either positive or negative slope. This insures that the condensate will flow the condenser to the lowest portion of the evaporator.

Hairpin thermosyphon: To eliminate the unsightly collision hazard on the roadway the condenser part is also buried under the ground along with the evaporator part. In addition, in between the condenser and evaporator sections there is an insulation layer is present to inhibit the heat flowing directly to the condenser portion.
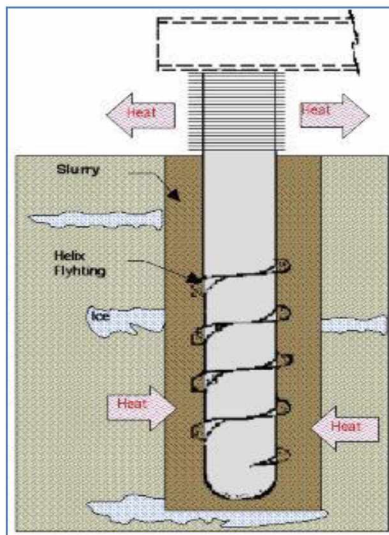
(a)   (b)
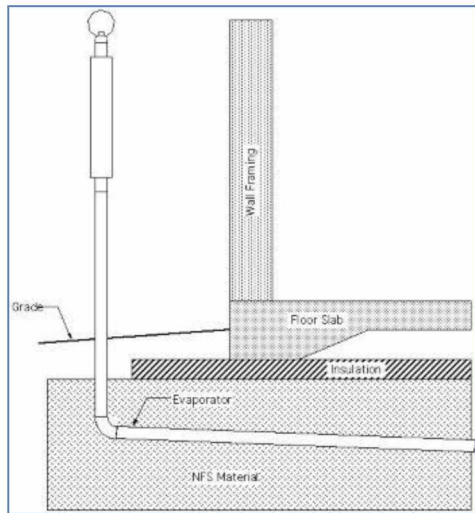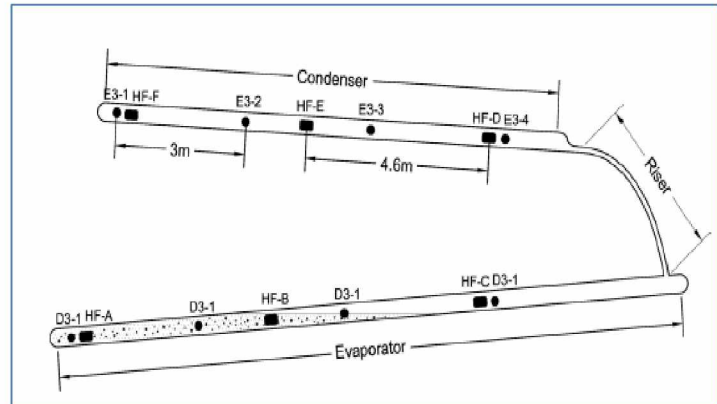
(C)   (d)

Figure: 1.7: Different Thermosyphon designs (a) Themopile (b) Thermoprobe (c) Sloped Thermosyphon (d) Hairpin Thermosyphon [8]

1.3   Application 2: Metal hydrides for hydrogen energy storage

Hydrogen energy is a part of the green energy transition and it can serve as a key part in the effort to replace fossil fuels. Hydrogen can be produced from various sources including water, natural gases and other hydrocarbons. Global climatic changes as the green house effect shows adverse consequences on the environment caused by the usage of fossil fuels. Storage of hydrogen energy is a difficult task, and a lot of research is underway in this area to store the energy in the best possible manner in terms of safety. Figure 1.8 show below gives a basic idea about the hydrogen storage technologies. Hydrogen storage is of two types; physical and material-based storage systems. Physical storage consists of storage as a compressed gas under a pressure range of (300~500 psi), which is a high pressure with associated saftey issues. Another physical storage option is cryogenic storage which involves keeping the hydrogen in a liquid state and maintaining temperature at 20.28 K. It is a challenging task to retain such a low temperature and moreover it is a costly method generally reserved for space missions.

Another approach, material based storage, is the preferred method for hydrogen storage in terms of safety related issues. Metal hydrides are a promising material for hydrogen storage, where hydrogen is stored in metal form. Operation of the metal hydride is a simple process which is illustrated in Figure 1.9. Initially, there is an equilibrium pressure range which holds the hydrogen in the metal hydride powder. The charging process begins when hydrogen pressure is greater than the equilibrium pressure. Hydrogen charging is an exothermic reaction, where heat is released during the chemical reaction. The discharging process activates when hydrogen pressure is lower than the equilibrium pressure, and is endothermic.
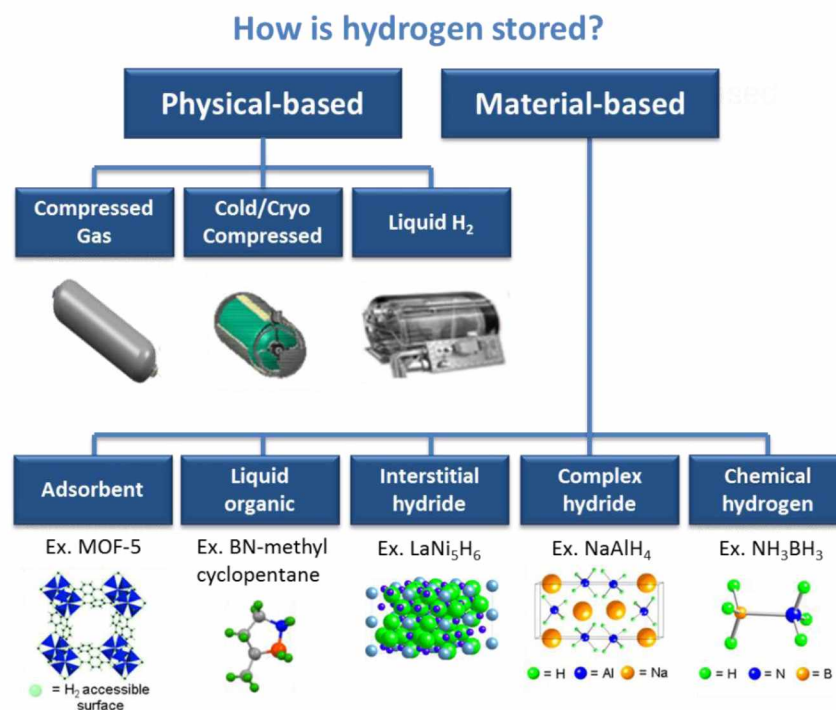
Figure: 1.8: Hydrogen Energy storage Techniques [9]
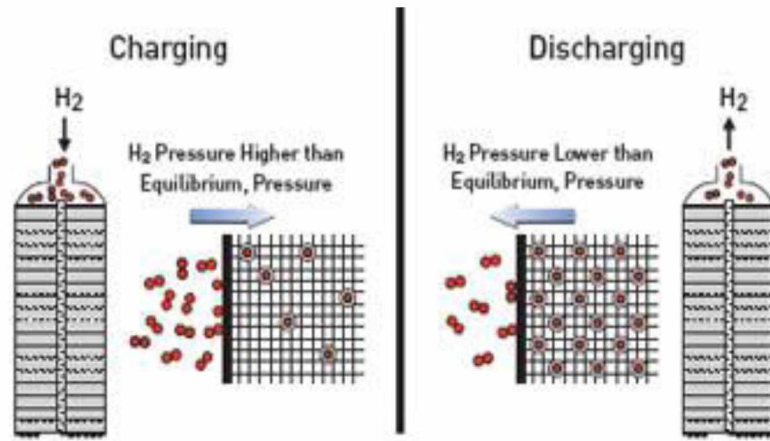
1.4   Objective

Thermosyphons are the best passive cooling devices used for protecting surface facilities in thawing permafrost. However, there is no research done in optimal spacing between two thermosyphons for effective cooling performance. And in this reserch we mainly concentate on the evaporator section of the thermosyphon, we design evaporator section into different geometrical structures as Y-shape, T-shape with different bifurcation levels and compare with the classical design (parallel shaped evaporator). A mathematical model was developed in COMSOL™ to simulate the optimal spacing and best performance of the different evaporator designs. Hydrogen is the one of the abundant available green energy, however storing hydrogen is one of the difficult tasks. There is lot of research ongoing on hydrogen energy storage and metal hydrides are one of the promissing materials for hydrogen energy storage. And a COMSOL™ model is developed for reducing the hotspots and rapid hydrogen absorption in the Metal hydride model.

1.4.1 Scope of the dissertation

A literature review related to the metal hydrides and constructal law is given in Section to follow. Validation model and results of thermosyphon with tree shaped structures using

13

constructal law are modeled in COMSOL™ are presented in Chapter 2. A mathematical model of metal hydride reactors for hydrogen energy storage are modeled ard expressed detail in Chapters 3&4. Chapter 5 consists of general conclusions.

1.5 Literature review

A lot of research is being done on to find the optimized design which best suits the structure. Design with the constructal theory offers a innovative new approach based on the physics for understanding and predicting the designs which arise in the nature and engineering, from atree structure to cooling of electronics, vascular smart materials, under ground heat pumps design. It has been only over fifteen years from the birth of the constructal theory now, however it's reserch applications have covered from electricity, magnatisam, heat exhange, physics, chemistry and other disciplines in the engineering, to the animate systems in the nature and its organs, and moreover, in-animate systems such as river basins, climate change, architectural design, ocean currents, and many other fields, and productive achivements have been obtained. Below are the few noval methods tried to find the best optimized flow structure using constructal theory.

1.5.1 Constructal design in nature, biology, geophysics, to engineering

The applications of constructal theory in engineering have a wide range of research-related contents. Encompassing, but not limited to, the fields of fluid flow, heat conduction, convective heat and mass transfer, performance optimization of devices such as insulation walls, fuel cells, solar energy devices, solid-state bioreactors, heat exchangers, refrigeration equipment, thermoelectric devices, etc. These research topics are continuously being developed and further imporved upon, along with more general, classically-related issues such as heat conduction, convective heat transfer, and fluid flow.

14

Optimization of many aspects of the above-related topics focus chiefly on single and multi-objective topics. For example, concerns such as minimum and maxiumum heat transfer rate, entropy generation rate, thermal resistance, exergy loss rate, heat density, flow resistance and the like can all be considered as viable objectives for optimization techniques. In order to solve for such objectives, increasingly complex solution methods have been developed, such as numerical optimization techniques coupled with mathematical and physical modeling which mirror the experimental results achieved in the laboratory.

The constructal law has the vast number of applications among them the design from the nature, as animate systems such as design structure of lungs and inanimate systems such as water flow, the water takes the path of mimimal flow resistance in joining into river basin. Constructal law describes the tree structure, as the tree has evolving from the millions of years to get the optimal shape as to provide the nutrients and fluid transport to all of its branches from the ground. As in this way this philosophy was applied to all flow systems in the nature, from biology, physics, trees, to engineering applications [11-20].

In medicine [21,22], the constructal law is applied to treat cancer. In hyperthermia cancer treatments, the main problem is to maintain the temperature of the normal tissue in a threshold limit so as to prevent the damage to that tissue from the abnormal cancer tissue. The parameters and the blood flow of the multi level blood vessels are determined based on the constructal law. In heat transfer conduction [23,24] the application ranges from electronic cooling, mimimizing hotspot of a system etc. In the electronic cooling, a lot of research is going on in the thermal management of the electronic circuits in order for high performance and reliability of the electronics system.

In heat convection [25,26], a lot of research is going on in determining of the optimal spacing of the array of the cylinders for the effective natural convection. And in fluids [27-32],

Adrian bejan proposed fluid flow resistance can be minimized by optimizing the internal flow architectures in different design configurations.

1.5.2 Thermosyphon applications in permafrost zone

Thermosyphon [33-36] is bassically a passive phase change heat transfer device, and widely used in Alaska and other Northern regions to facilitate stability to the foundations in the permafost zones. The orientation of the thermosyphon is of vertical orientation, used for pipeline stability, and in a horizontal alignment, as under roads, buildings, airport structures. While constructing the embankments on the permafrost zones they may induce substamcial disturbance on the heat and mass transfer energy balance between the ground and the atmosphere, which results in disturbance in the energy balance and more amount of heat is absorbed in to embankment. As a result, the temperature of the permafrost underneath the ground raise, this may lead to thawing of permafrost. Under this consideration, to protect the surface facilities from the permafrost, there are numorous methods such as thermal insulation, ventilated embankment, awnings are employed. However, these all methods have certain limitations, for instance, anny blokage of debris in the ventiduct embankment leads to misfunction.

1.5.3 Metal hydride applications

Metal hydrides are the combination of metal and alloy [37,38]. $LaNi_5$, MgH_2, and $NaAlH_4$ are few examples of metal hydrides, can be used as a storage medium for hydrogen. There is a set equilibrium pressure at that state the hydrogen is neither released nor absorbed. The equilibrium pressure sets an equlibrium temperature, we need to supply heat in order to release hydrogen from metal hydride and if the temperature falls below the equilibrium pressure the hydrogen is absorbed in to the metal hydride.

1.5.4 References

[1] Adrian Bejan and Sylvie Lorente, Design with constructal theory, John Wiley sons, Inc. 2008, Hoboken, New Jersey ISBN: 978-0-471-99816-7

[2] http://www.science blogs.com, accessed on 02/01/2016

[3] http://www.nicolelbates.com, accessed on 02/01/2016

[4] Muller, S. (1943). Permafrost or permanently frozen ground and related engineering problems. U.S. Engineers Office, Intelligence Branch, Strategic Engineering study report 62.

[5] US Geological Survey

[6] Rail Embankment Stabilization on Permafrost – Global Experiences a report by Shane M. Ferrell & Pasi T. Lautala, 2010

[7] http://www. thermalfluidscentral.org, accessed on 02/01/2016

[8] http://www.arcticfoundations.com/index.php/technologies, accessed on 02/01/2016

[9] http://www.energy.gov, accessed on 05/03/2016

[10] http://www.1-act.com, accessed on 05/03/2016

[11] A. Bejan, Why the bigger live longer and travel farther: animals, vehicles, rivers and the winds, Sci. Rep. 2 (2012) 1–5. doi:10.1038/srep00594.

[12] A. Bejan, Constructal Thermodynamics, Int. J. Heat Technol. 34 (2016) S1–S8. doi:10.18280/ijht.34S101.

[13] A. Bejan, S. Lorente, The constructal law and the evolution of design in nature, Phys. Life Rev. 8 (2011) 209–240. doi:10.1016/j.plrev.2011.05.010.

[14] A. Bejan, S. Lorente, Constructal law of design and evolution: Physics, biology, technology, and society, J. Appl. Phys. 113 (2013). doi:10.1063/1.4798429.

[15] A. Bejan, G.W. Merkx, Constructal Theory of social dynamics, 2007. doi:10.1007/978-0-387-47681-0.

[16] S. Lorente, E. Cetkin, T. Bello-Ochende, J.P. Meyer, a. Bejan, The constructal-law physics of why swimmers must spread their fingers and toes, J. Theor. Biol. 308 (2012) 141–146. doi:10.1016/j.jtbi.2012.05.033.

[17] A.F. Miguel, Constructal pattern formation in stony corals, bacterial colonies and plant roots under different hydrodynamics conditions, J. Theor. Biol. 242 (2006) 954–961. doi:10.1016/j.jtbi.2006.05.010.

[18] a. H. Reis, Constructal view of scaling laws of river basins, Geomorphology. 78 (2006) 201–206. doi:10.1016/j.geomorph.2006.01.015.

[19] a. H. Reis, C. Gama, Sand size versus beachface slope - An explanation based on the Constructal Law, Geomorphology. 114 (2010) 276–283. doi:10.1016/j.geomorph.2009.07.008.

[20] S. Ziaei, S. Lorente, a. Bejan, Morphing tree structures for latent thermal energy storage, J. Appl. Phys. 117 (2015). doi:10.1063/1.4921442.

[21] a H. Reis, a F. Miguel, M. Aydin, Constructal theory of flow architecture of the lungs., Med. Phys. 31 (2004) 1135–1140. doi:10.1118/1.1705443.

[22] H. Wang, W. Dai, A. Bejan, Optimal temperature distribution in a 3D triple-layered skin structure embedded with artery and vein vasculature and induced by electromagnetic radiation, Int. J. Heat Mass Transf. 50 (2007) 1843–1854. doi:10.1016/j.ijheatmasstransfer.2006.10.005.

[23] A. Bejan, M. Almogbel, Constructal T-shaped fins, Int. J. Heat Mass Transf. 43 (2000) 2101–2115. doi:10.1016/S0017-9310(99)00283-5.

[24] Q. Xiao, L. Chen, F. Sun, Constructal optimization for "disc-to-point" heat conduction without the premise of optimized last-order construct, Int. J. Therm. Sci. 50 (2011) 1031–1036. doi:10.1016/j.ijthermalsci.2011.01.016.

[25] T. Bello-Ochende, a. Bejan, Constructal multi-scale cylinders with natural convection, Int. J. Heat Mass Transf. 48 (2005) 4300–4306. doi:10.1016/j.ijheatmasstransfer.2005.05.023.

[26] S. Lorente, a. Bejan, Svelteness, freedom to morph, and constructal multi-scale flow structures, Int. J. Therm. Sci. 44 (2005) 1123–1130. doi:10.1016/j.ijthermalsci.2005.08.011.

[27] A. Bejan, Constructal tree network for fluid flow between a finite-size volume and one source or sink, Rev. Générale Therm. 36 (1997) 592–604. doi:10.1016/S0035-3159(97)89986-2.

[28] K.H. Cho, J. Lee, H.S. Ahn, A. Bejan, M.H. Kim, Fluid flow and heat transfer in vascularized cooling plates, Int. J. Heat Mass Transf. 53 (2010) 3607–3614. doi:10.1016/j.ijheatmasstransfer.2010.03.027.

[29] S. Kim, S. Lorente, a. Bejan, Transient behavior of vascularized walls exposed to sudden heating, Int. J. Therm. Sci. 48 (2009) 2046–2052. doi:10.1016/j.ijthermalsci.2009.03.019.

[30] S. Kim, S. Lorente, a. Bejan, W. Miller, J. Morse, The emergence of vascular design in three dimensions, J. Appl. Phys. 103 (2008). doi:10.1063/1.2936919.

[31] S. Kim, S. Lorente, A. Bejan, Vascularized materials: Tree-shaped flow architectures matched canopy to canopy, J. Appl. Phys. 100 (2006). doi:10.1063/1.2349479.

[32] J. Lee, S. Kim, S. Lorente, a. Bejan, Vascularization with trees matched canopy to canopy: Diagonal channels with multiple sizes, Int. J. Heat Mass Transf. 51 (2008) 2029–2040. doi:10.1016/j.ijheatmasstransfer.2007.06.015.

[33] F.D. Haynes, J.P. Zarling, G.E. Gooch, Performance of a thermosyphon with a 37-meter-long, horizontal evaporator, Cold Reg. Sci. Technol. 20 (1992) 261–269. doi:10.1016/0165-232X(92)90033-Q.

[34] R.M. Bayasan, A.G. Korotchenko, N.G. Volkov, G.P. Pustovoit, A.D. Lobanov, Use of two-phase heat pipes with the enlarged heat-exchange surface for thermal stabilization of permafrost soils at the bases of structures, Appl. Therm. Eng. 28 (2008) 274–277. doi:10.1016/j.applthermaleng.2006.02.022.

[35] J. Wu, W. Ma, Z. Sun, Z. Wen, In-situ study on cooling effect of the two-phase closed thermosyphon and insulation combinational embankment of the Qinghai-Tibet Railway, Cold Reg. Sci. Technol. 60 (2010) 234–244. doi:10.1016/j.coldregions.2009.11.002.

[36] G. Cheng, Z. Sun, F. Niu, Application of the roadbed cooling approach in Qinghai-Tibet railway engineering, Cold Reg. Sci. Technol. 53 (2008) 241–258. doi:10.1016/j.coldregions.2007.02.006.

[37] McWhorter, S.; O'Malley, K.; Adams, J.; Ordaz, G.; Randolph, K.; Stetson, N. T. Moderate Temperature Dense Phase Hydrogen Storage Materials within the US Department of Energy (DOE) H2 Storage Program: Trends toward Future Development. Crystals 2012, 2, 413–445.

[38] Felderhoff, M.; Bogdanović, B. High temperature metal hydrides as heat storage materials for solar and related applications. Int. J. Mol. Sci. 2009, 10, 325–344.

Chapter 2

Optimum configuration for roadway embankment stabilization on permafrost using constructal law

2.1   Abstract

Constructing surface facilities on permafrost soils is a substantial engineering challenge. In addition, evading the thaw-settlement on roadway embankments is not an easy task due to the shifting thermal regime under the ground soil in accordance with the seasonal temperature variations. Out of all engineered cooling solutions available to stabilize the permafrost soil, thermosyphons have attracted many researchers through its benefits compared to other cooling methods. The only limitation in their application for permafrost regions is their capital investment. If we can increase the efficiency of thermosyphons, we can reduce the total number required for each application. In the research outlined in this thesis, the optimization of thermosyphons is studied at length. Here, the constructal law approach is used to optimize the thermosyphons, which accounts for the universal tendency of freely morphing flow systems to generate configurations that evolve toward greater access for their currents. We compared the cooling effects and found the optimal spacing between thermosyphons for both parallel evaporator and the bifurcated evaporator (T, Y sections) configurations. The ideal bifurcation level was found, and then was further analyzed for the cooling effects of different bifurcated level models.

Nomenclature

D	pipe diameter, m
L	pipe length, m
T	temperature, K
V	volume, m^3
t	time, s
N	bifurcation level
x, y, z	coordinates, m
W	width, m
T_p	pipe temperature, K
T_s	Solid temperature, K

Greek symbols

α	thermal diffusivity, m^2s^{-1}
γ	bifurcation angle
θ	dimensionless temperature
φ	volume fraction

Subscripts and superscripts

avg	average
*	dimensionless
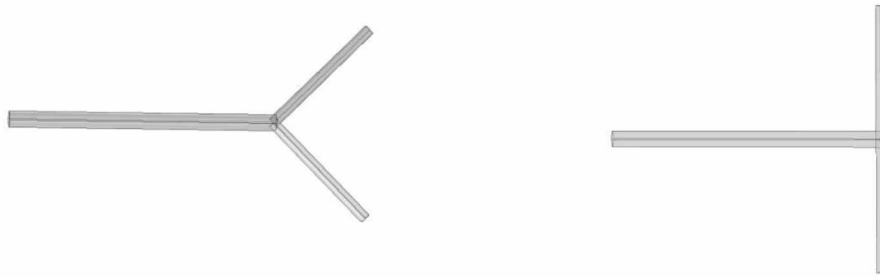
Figure 2.1: Y and T shaped structures

2.2   Introduction

Permafrost is a soil at or below the freezing point of water ($0°C$) for duration of two or more years. Permafrost soil is a major obstacle in high latitude regions such as the Arctic and Antarctic as this soil tends to thaw due to the shifting thermal regime. Stabilizing the thaw-settlements on the roadway embankments in the permafrost zones is a highly technical engineering challenge. Roadway embankments are one of various engineering structures that contribute to failure due to thawing permafrost. Roadway embankments constructed in the permafrost zones have shifting thermal regime since they modify ground surface energy balance. Due to this shifting thermal regime, permafrost thaws with respect to seasonal variations, this contributes to loss of potency in foundation soil. This causes failure and instability of embankment results in outward movement of bottom side embankment. The ground surface energy balance of the embankment mainly depends on numerous factors such as radiation, atmospheric air temperature, flora, etc. These factors influence the mean average surface temperature (MAST), and therefore it can differ from the mean average air temperature (MAAT). Due to this differential variation in thermal regime occurring in the ground, this often times results in thawing permafrost under roadway embankments.

Thermosyphon cooling is one of the passive cooling methods, which is widely used in cold regions to evade thaw-settlement in the permafrost soil [1–5]. The condenser and the evaporator are components within the thermosyphon, where the working fluid is circulated between the two parts. Our main interest in this research is the evaporator, which is buried in the soil at a certain known depth. When the ground is heated due to shifting thermal regime, the working fluid in the evaporator changes its phase from liquid to vapor, which rises up to the condenser section. In the condenser, the heat is rejected outside, where the vapor cools and condenses along the wall; then the working fluid then moves down to the evaporator section and this cycle continues. This process is thus driven both by the gravity and the temperature difference. There is a growing interest in designs which have the potential to improve the performance of the evaporator section in the thermosyphons. The classical design of the evaporator section in the thermosyphon consists of pipes arranged in a simple parallel geometry, and this design has been used widely in previous research [2,6,7]. In the research discussed here, we employ the constructal law to improve the parallel evaporator.

The design of the flow structure in nature and engineering is governed by the principals of constructal law. Bejan has stated, "For a finite-size flow system to persist in time (to live), its configurations must change in time such that it provides easier and easier access to its currents (fluid, energy, species, etc.)" [8–12]. Constructal theory encompasses a wide range of space in the "design" drawing from each end every field from engineering to biology. The universal design of nature and the constructal law unify all animate schemata such as human blood circulatory systems, and inanimate systems, such as urban traffic and river basins. Research is mainly focused in designing different types of the flow architectures, which offer a greater accessibility of the flow in between a sink and a defined volume. Current progress and assessments made by the constructal law in various fields from engineering to geophysics and

biology are provided in References [13–17]. In this research we propose tree-shaped designs (Y-shape) and T-shaped tree designs for the evaporator section (Figure 2.1). Furthermore, in this paper we compare the evaporator performance for the different configurations: Y-shaped trees, T-shaped trees, and classical designs (parallel evaporator case). The net volume occupied by all the pipes is fixed in all the configurations. Therefore, the volume fraction (φ) occupied by all the pipes inside the conduction zone is equal. The tree structures with Y-shaped and T-shaped designs grow their configurations with respect to the bifurcation levels (N). The classical design (parallel shaped structure) diameter is increased step by step, in order to maintain the constant value of volume fraction (φ) for all the designs.

2.3 COMSOL™ Validation model

To validate our computational model, we modeled the numerical simulations of Dr. Bejan's "Double tree structures in a conducting body" [18] and verified the results with our inbuilt model and found 100% agreement with results, as indicated in figure 2.8. Figure 2.6 represents a 1st level Y shaped bifurcation tree shaped structure used in ground source heat pump models. Our task is to model the 1st level Y shaped bifurcation in Comsol, and to verify if the results produce the same graph as Bejan's (figure 2.6). Figure 2.8 plots volume average temperature against spacing and shows good agreement with Bejan's model.

Figure 2.7 represents temperature distribution for 1st level bifurcation tree shaped structures at a non-dimensionalized time value of one. Additionally, shown in figure (2.2) below is the Comsol™ model with level 4 bifurcation "Y" shape tree structures for a GSHP model. Figure 2.3 represents Dr. Bejan's optimized angles for each bifurcation level.
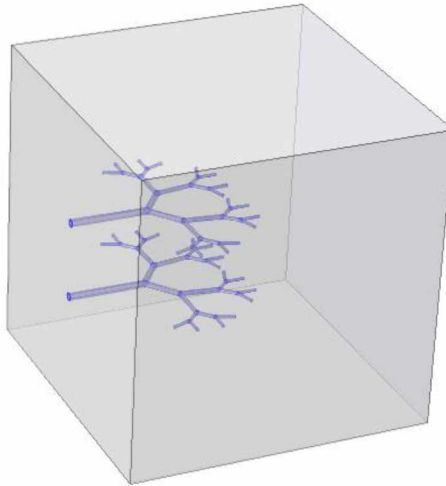
Figure 2.2: Comsol™ built in "Y" structured model
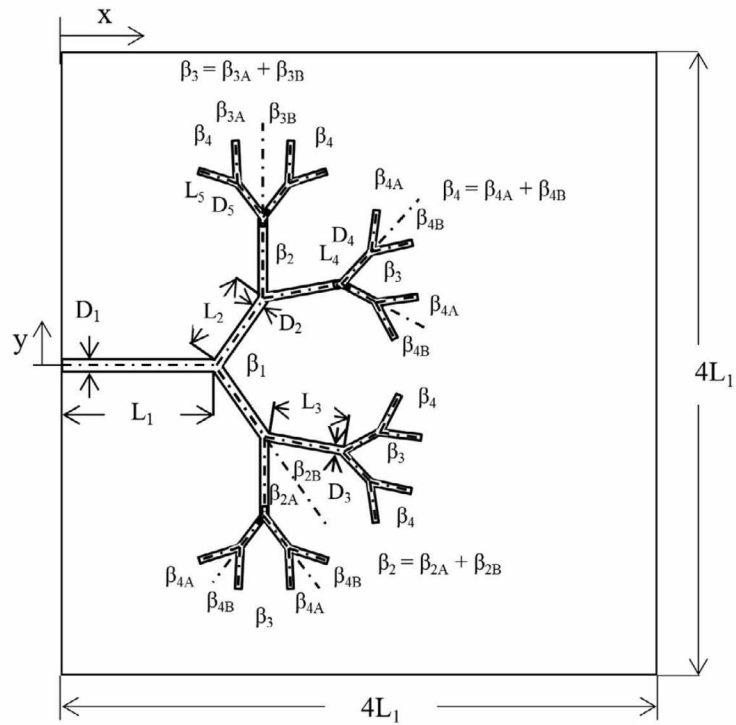
Figure 2.3: Bejan's [18] optimized angles

$\beta_1 = 105° \quad \beta_2 = 82°$
$(\beta_{2A} = \beta_{2B} = 41°)$
$\beta_3 = 85°$
$(\beta_{3A} = \beta_{3B} = 42.5°)$
$\beta_4 = 70°$
$(\beta_{4A} = 40° \quad \beta_{4B} = 30°)$
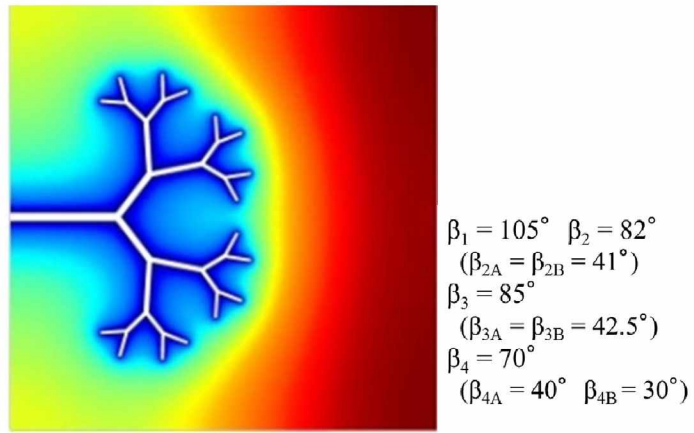
Figure 2.4: Temperature distribution of bifurcation level 4 Y structure
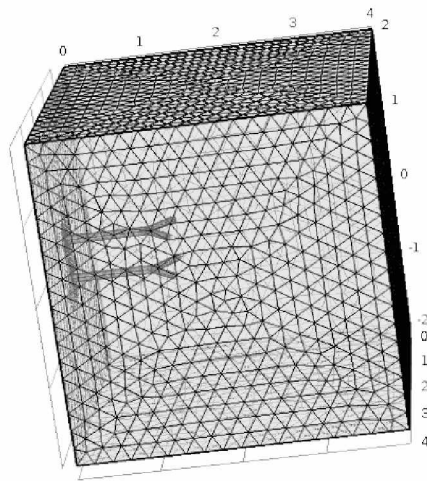
Figure 2.5: 1st level Y shaped bifurcation
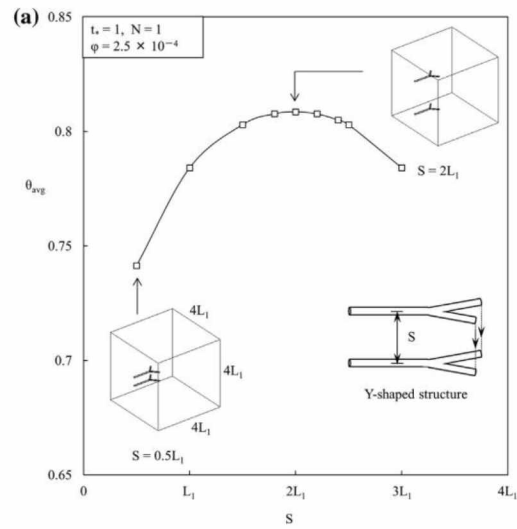
Figure 2.6: Dr. Bejan's Y shaped tree first bifurcation
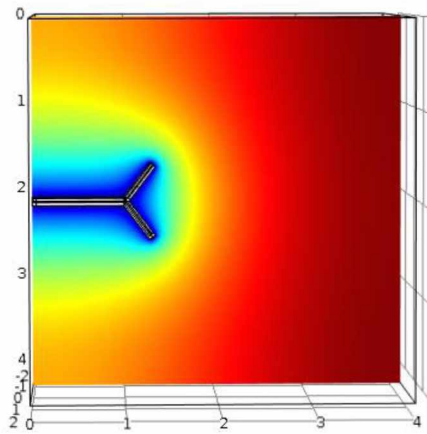
Figure 2.7: Temperature distribution @ t* =1
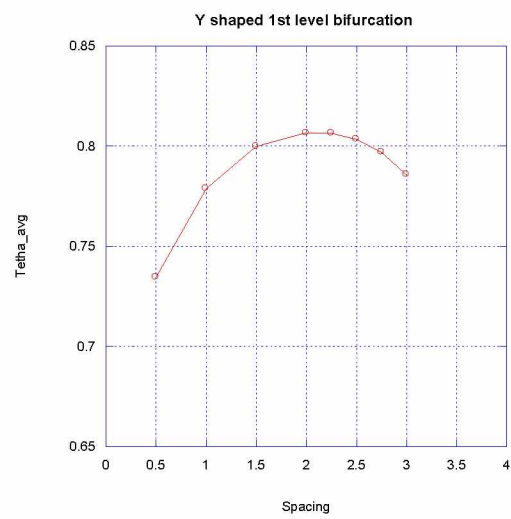
Figure 2.8: Comsol™ model Y shaped tree first bifurcation

2.4 Mathematical model and methods

The geometry of the roadway embankment model is adopted from a highly cited paper [18]. The dimensions associated with a typical embankment are illustrated in Figure 2.9. This model consists of a highway embankment with driving surface width of 6 m and height of 2.5 m. The lower boundary is 9 m beneath the pavement surface, and the outer vertical boundary is 17 m from the centerline (C_L). Due to the symmetry we only considered the half portion of the model. We are interested in finding the optimal spacing between two neighboring thermosyphons by minimizing the volume averaged temperature. That is, we will consider that the road is of infinite length and that the thermosyphons are installed equidistantly. By varying the width of the model and finding the minimum volume averaged temperature, the width itself is then optimal spacing. The pipe links of the tree structure are modeled as isothermal, which are buried in the solid at a different temperature. This assumption is reasonable because the flow in the pipes is intense and the convective heat transfer coefficient in the pipes is very high. The total volume of the solid medium is V= 124.25 X W, where W is the width of the model. The boundary of the entire volume is modeled as adiabatic. The solid is initially at temperature (T_s), which is higher than the temperature of the pipes (T_p). In time due to the temperature difference, a heat transfer occurs between the solid ground and the pipes and a cooled zone grows around the cylinders.

The tree structure is an assembly of the Y and T shaped bifurcations. The lengths of the branches are modeled in the sequence shown in Figure 2.1.

$$L_1 = 3m, L_2 = \frac{L_1}{3}, L_3 = L_2, L_4 = \frac{L_3}{3} \tag{2-1}$$
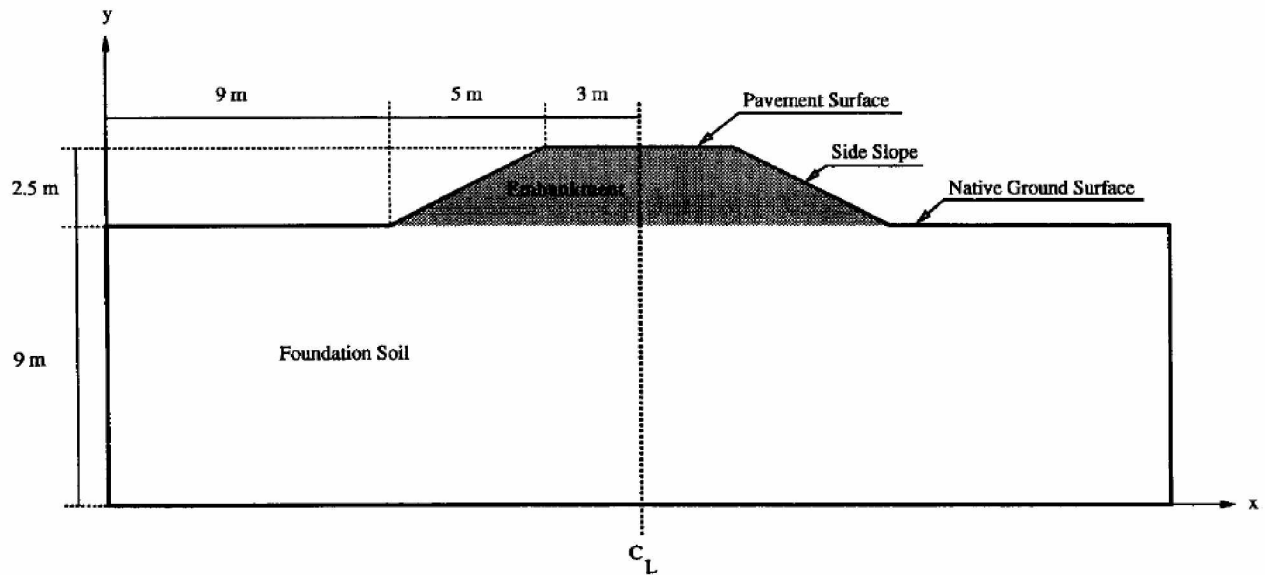
Figure 2.9: Model embankment geometry [18]
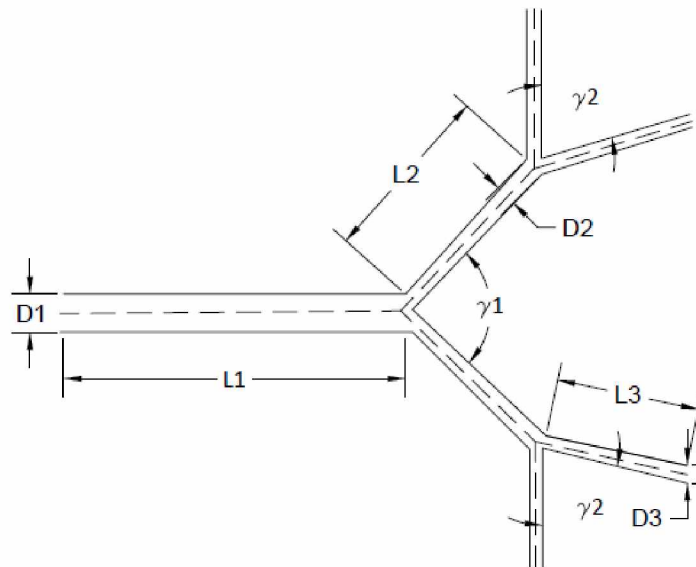
Figure 2.10: Tree structure lengths and branch angles

All of the pipe's cross sections are round, mirroring the real-world design in which accommodates the fluid flow, such as with the working fluid of the thermosyphon. The minimization of the fluid flow resistance calls for a particular sequence of the diameter sizes, and the round shape holds for both laminar and turbulent flow regimes. For the laminar zone the

29

diameter of the pipes are sized relative to one another in according to Hess-Murray rule [8],

$$\frac{D_i}{D_{i+1}} = 2^{1/3} \ (i=1,2,3...)$$ (2-2)

The lengths of the branches of the evaporator are equal for both T-shaped and Y-shaped bifurcations, Eq. (1). We allow Y-shaped branches to freely morph the first bifurcation angle between the trunks, wherein the pipe branch is denoted as γ_1. The second, third and fourth angle bifurcations are similarly denoted as the γ_2, γ_3, γ_4, etc.

The heat transfer process was simulated as transient heat conduction by using the commercially available computational package, COMSOL™ [19]. The conservation of energy in the solid that surrounds the branch structures is governed by

$$\frac{\partial T}{\partial t} = \alpha \nabla^2 T$$ (2-3)

α is the thermal diffusivity of the solid. And, $\nabla^2 = \frac{\partial^2}{\partial x^2} + \frac{\partial^2}{\partial y^2} + \frac{\partial^2}{\partial z^2}$, where x, y, z are the coordinates of the model. For greater generality, we determine the temperature field in terms of the dimensionless variables.

$$(x_*, y_*, z_*) = \frac{x, y, z}{V^{1/3}}$$ (2-4)

$$t_* = \frac{\alpha t}{V^{2/3}}$$ (2-5)

$$\theta = \frac{T_p - T}{T_p - T_s}$$ (2-6)

Eq. (3) can be written in terms of the dimensionless variables as

$$\frac{\partial \theta}{\partial t_*} = \frac{\partial^2 \theta}{\partial x_*^2} + \frac{\partial^2 \theta}{\partial y_*^2} + \frac{\partial^2 \theta}{\partial z_*^2} \qquad (2\text{-}7)$$

And the initial boundary conditions are

$$\frac{\partial \theta}{\partial x_*} = 0 \ at \ x_* = 0, 17 \ \frac{\partial \theta}{\partial y_*} = 0 \ at$$

$$y_* = 2, -6 \ \frac{\partial \theta}{\partial z_*} = 0 \ at \ z_* = 0, W \qquad (2\text{-}8)$$

$$\theta = 1 \ at \ t_* = 0 \qquad (2\text{-}9)$$

2.4.1   Volume averaged temperature

Initially we start the simulation from $t_*= 0$ seconds, where the heat is transferred from the solid to the pipes (tree-shaped). We are interested in finding the effective volume averaged temperature with different bifurcated tree structures. As the t_* value increases, the volume averaged temperature of the cube approaches that of the pipe temperature (T_p). Here we are interested in finding out the thermal equilibrium with respect to the different tree geometries. In this process we are studying the heat transfer process by fixing the non-dimensionalzed time ($t_*=1$), and finding out the effective averaged temperature (θ_{avg}) at that instant.

$$\theta_{avg} = \frac{T_p - T_{avg}}{T_p - T_s} \qquad (2\text{-}10)$$

2.4.2   Bifurcation angles

We are trying to find out the effective volume averaged temperature (θ_{avg}) by using the different tree shaped configurations. In this research we are modeling at maximum two bifurcation levels. The first bifurcation angle is the branch divided from the end point of the

trunk part. And the angle is maintained at $\gamma_1 = 90°$ for Y shaped architecture. In T shaped architecture the angle is of $\gamma_1 = 180°$ and, both angles are held constant for each and every bifurcation.

2.5 Comparing the tree structures with the classical model

From the beginning bifurcation level, the tree shaped structures perform much better than the classical evaporator model. We compared the heat transfer performance of the Y, T shaped designs and classical evaporator model with same porosity and bifurcation levels. The volume-averaged temperature (θ_{avg}) is shown in (Figure 2.11 and 2.12) for first and second level bifurcations.
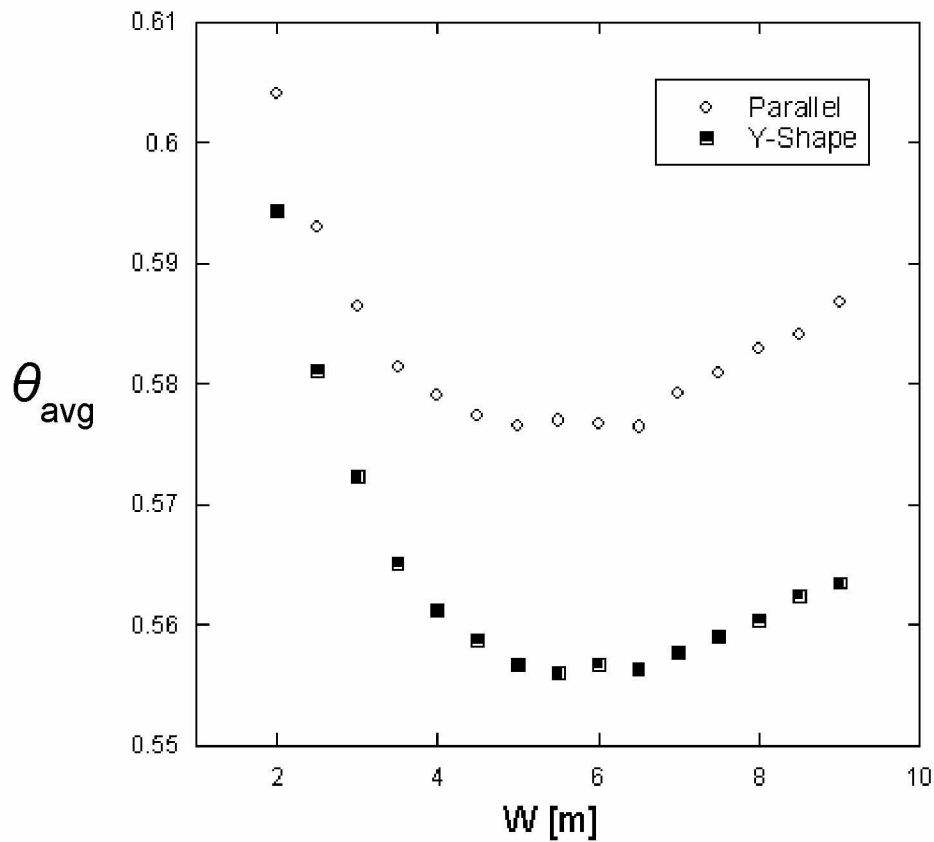
Figure 2.11: Comparison of volume averaged temperature with respect to width for Y and classical shaped evaporator for 1st bifurcation.

32
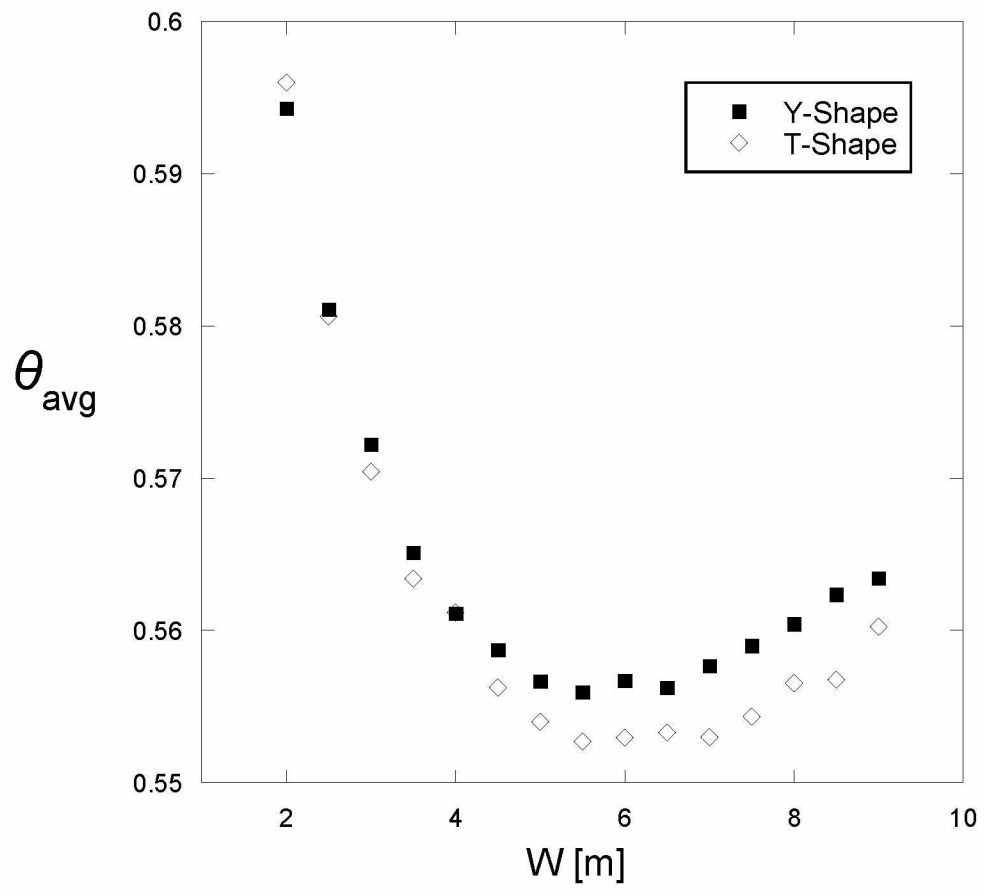
Figure 2.12: Comparison of volume averaged temperature with respect to width for Y and T shaped evaporator for 1st bifurcation.

2.6   Finding the optimal spacing for the model

We found that the tree shaped configurations perform much better than the existing classical design shown in (Figure 2.11). The optimal spacing is dependent on the bifurcation level, as we maintained the same volume fraction (porosity) between each model i.e. $3X10^{-5}$. For the first bifurcation level the optimum spacing is found at 5.5 m width as shown in Fig. 2.12 and 2.17. In this model, volume averaged temperature (θ_{avg}) for Y shape and T shaped structures are close enough until 4m width. From 4 m width, the T-shaped architecture shows a minimum (θ_{avg}). For the second bifurcation level, Y-shaped architecture leads from the

beginning width as shown in Fig. 2.13 and 2.15. The optimal spacing for the second bifurcation level is found at 7 m.
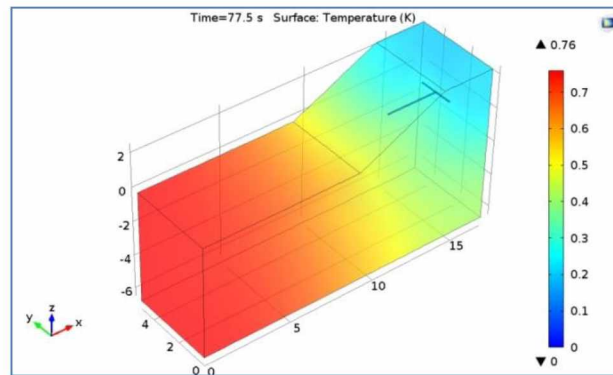
Figure 2. 14: optimum spacing for 1st bifurcation level T-shape
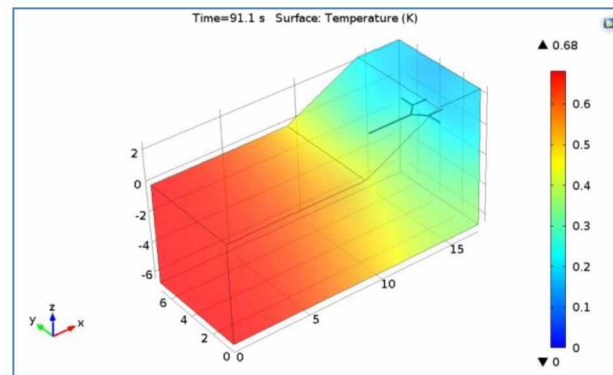
Figure 2.15: optimum spacing for 2nd bifurcation level Y-shape
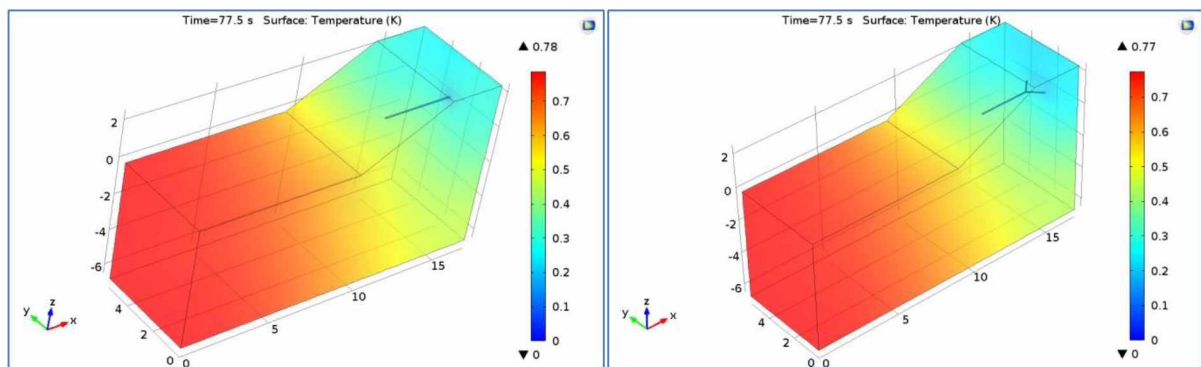
Figure 2.16&17: Comsol™ model comparison at optimum width (5.5 m) for 1st bifurcation Y and classical shaped architectures

35
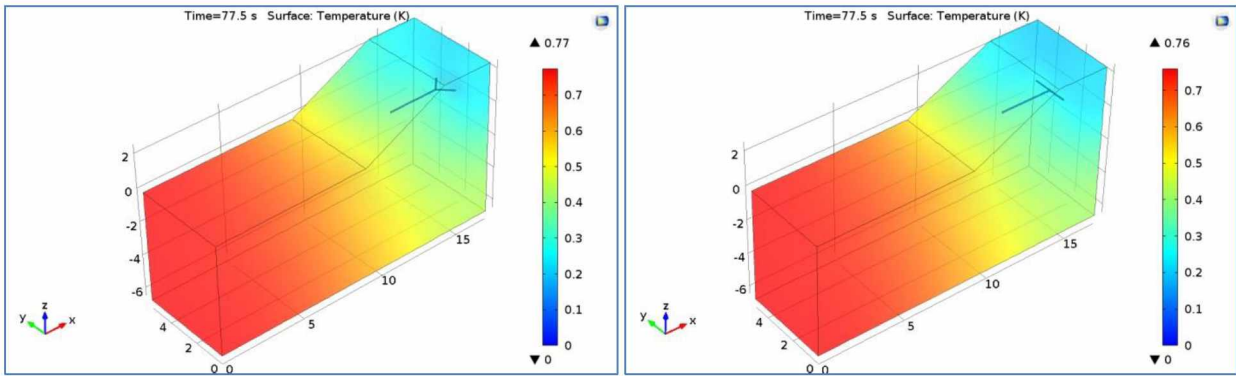
Figure 2.18& 19: Comsol™ model comparison at optimum width (5.5 m) for 1st bifurcation Y and T shaped architectures
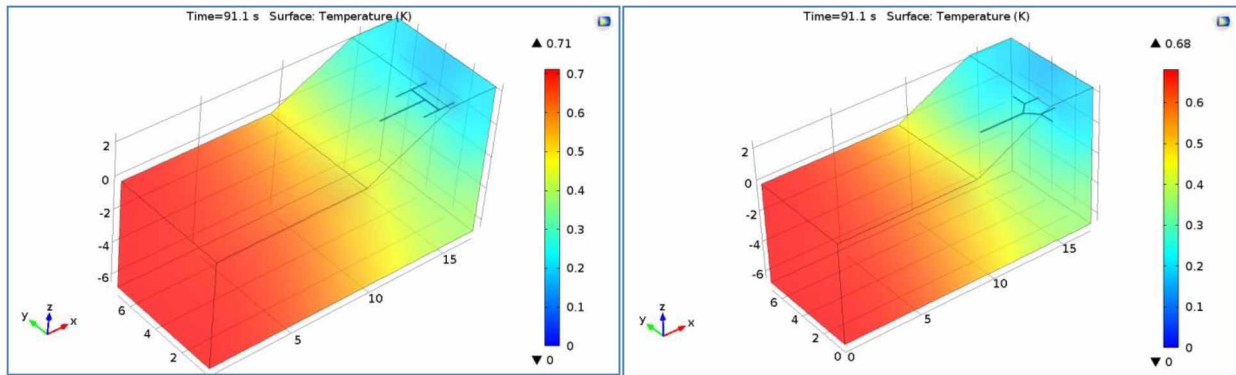
Figure 2.20&21: Comsol™ model comparison at optimum width (7 m) for 2st bifurcation Y and T shaped architectures

2.7 Conclusions

In this research, we developed tree shaped configurations to study the heat transfer performance against the existing classical evaporator model. We successfully analyzed the thermal performance of an architecture located in a conducting medium with different bifurcation levels.

The minimal volume averaged temperature is found in the T-structure for the first bifurcation when compared to Y shaped and classical evaporator designs. While coming to the

second bifurcation level, Y shaped architecture shows improved performance when compared to T shaped structures.

The optimal spacing of the evaporator is decided from the minimum volume averaged temperature as shown in Fig 2.14 and 2.15. The optimal spacing differs with different bifurcation level. The optimal spacing for the first bifurcation resulted in the T shaped structure, which was 5.5 m, then for the second bifurcation level, 7 m resulted in the Y shaped structure.

2.8 References

[1]   W. Zhi, S. Yu, M. Wei, Q. Jilin, J. Wu, Analysis on effect of permafrost protection by two-phase closed thermosyphon and insulation jointly in permafrost regions, Cold Reg. Sci. Technol. 43 (2005) 150–163. doi:10.1016/j.coldregions.2005.04.001.

[2]   J. Wu, W. Ma, Z. Sun, Z. Wen, In-situ study on cooling effect of the two-phase closed thermosyphon and insulation combinational embankment of the Qinghai-Tibet Railway, Cold Reg. Sci. Technol. 60 (2010) 234–244. doi:10.1016/j.coldregions.2009.11.002.

[3]   G. Cheng, Z. Sun, F. Niu, Application of the roadbed cooling approach in Qinghai-Tibet railway engineering, Cold Reg. Sci. Technol. 53 (2008) 241–258. doi:10.1016/j.coldregions.2007.02.006.

[4]   Y. Song, L. Jin, J. Zhang, In-situ study on cooling characteristics of two-phase closed thermosyphon embankment of Qinghai-Tibet Highway in permafrost regions, Cold Reg. Sci. Technol. 93 (2013) 12–19. doi:10.1016/j.coldregions.2013.05.002.

[5]   J. Xu, D.J. Goering, Experimental validation of passive permafrost cooling systems, Cold Reg. Sci. Technol. 53 (2008) 283–297. doi:10.1016/j.coldregions.2007.09.002.

[6]   F.D. Haynes, J.P. Zarling, G.E. Gooch, Performance of a thermosyphon with a 37-meter-long, horizontal evaporator, Cold Reg. Sci. Technol. 20 (1992) 261–269. doi:10.1016/0165-232X(92)90033-Q.

[7]   R.M. Bayasan, A.G. Korotchenko, N.G. Volkov, G.P. Pustovoit, A.D. Lobanov, Use of two-phase heat pipes with the enlarged heat-exchange surface for thermal stabilization of permafrost soils at the bases of structures, Appl. Therm. Eng. 28 (2008) 274–277. doi:10.1016/j.applthermaleng.2006.02.022.

[8]   A. Bejan, S. Lorente, Design With Constructal Theory, 1st ed., John Wiley & Sons, Inc., Hoboken, New Jersey, 2008.

[9]   A. Bejan, Advanced Engineering Thermodynamics, 2nd ed., Wiley, New York, 1997.

[10] A. Bejan, Constructal theory from engineering design to predicting shape and structure in nature, Engenharia Termica, n.1, 2001, P. 27-31.

[11] A. Bejan, M.R. Errera, Technology evolution, from the constructal law: heat transfer designs, Int. J. Energy Res. 39 (2015) 919–928. doi:10.1002/er.3262.

[12] a. Bejan, Constructal theory of pattern formation, Hydrol. Earth Syst. Sci. Discuss. 3 (2006) 1773–1807. doi:10.5194/hessd-3-1773-2006.

[13] A. Bejan, The constructal law of organization in nature: tree-shaped flows and body size., J. Exp. Biol. 208 (2005) 1677–1686. doi:10.1242/jeb.01487.

[14] A. Bejan, J.H. Marden, The constructal unification of biological and geophysical design, Phys. Life Rev. 6 (2009) 85–102. doi:10.1016/j.plrev.2008.12.002.

[15] C. Hadjistassou, a. Bejan, Y. Ventikos, Cerebral oxygenation and optimal vascular brain organization, J. R. Soc. Interface. 12 (2015) 20150245–20150245. doi:10.1098/rsif.2015.0245.

[16] a. Bejan, S. Lorente, R. Anderson, Constructal Underground Designs for Ground-Coupled Heat Pumps, J. Sol. Energy Eng. 136 (2013) 011019. doi:10.1115/1.4025699.

[17] H. Zhang, S. Lorente, A. Bejan, Vascularization with line-to-line trees in counterflow heat exchange, Int. J. Heat Mass Transf. 52 (2009) 4327–4342. doi:10.1016/j.ijheatmasstransfer.2009.03.064.

[18] D.J. Goering, P. Kumar, Winter-time convection in open-graded embankments, Cold regions Science and Technology, 24 (1996) 57–74.

[19] H. Kobayashi, a.Bejan, Double tree structure in s conducting body, 77(2014), International Journal of Heat and Mass Transfer 77 (2014) 140-146

[20]   http://www.comsol.com/. accessed on 05/06/2015

Chapter 3

Metal hydride reactor design optimization for hydrogen energy storage

3.1 Abstract

As hydrogen generation technologies using renewable energy sources are being developed, considerable attention is paid to storage and transportation of hydrogen gas. Metal hydride alloys are considered as promising materials because they are viewed as an attractive alternative to conventional hydrogen storage cylinders and mechanical hydrogen compressors. Compared to storing in a classic gas cylinder, which requires compression of hydrogen at high pressures, metal hydride alloys can store the same amount of hydrogen at nearly room pressure. However, this hydrogen absorption necessitates an effective way to reject the heat released from the exothermic hydriding reaction. In this paper, fin structures are employed to enhance the heat transfer of metal hydride alloys in a cylindrical reactor. Numerical simulations are performed based on a multiple-physics modeling to analyze the transient heat transfer during the hydrogen absorption process. The objective is to minimize the time elapsed for the process and to reduce the hotspot temperature by determining the number and shape of rectangular fins while the total volume of fins used are fixed. The simulations results show that the more fins are applied the better heat transfer is achieved and that there exists an optimal length of the fins.

3.2 Introduction

Metal hydrides are the binary combination of hydrogen and a metal or metal alloy. They can absorb a large amount of hydrogen through surface chemisorption and subsequent hydriding reactions. Because of their high uptake capacity of hydrogen, metal hydride alloys are viewed as an attractive alternative to conventional hydrogen storage cylinders and mechanical hydrogen compressors [1–5]. While storing hydrogen in a classic gas cylinder requires a significant amount of energy for compression of hydrogen at high pressures, metal hydride alloys store the same amount of hydrogen at nearly room pressure. However, this hydrogen absorption necessitates an effective way to reject the heat released from the exothermic hydriding reaction. One of the challenges is the poor thermal conductivity of metal hydride powder. Since the hydrogen absorption process (hydriding reaction of hydrogen with the metal alloy) involves a considerable amount of heat generation and since the temperature is a major factor in determination of the reaction rate, the heat must be effectively rejected out of the metal hydride reactor. The reversible reaction process can be expressed as

$$M + \frac{x}{2} H_2 \Leftrightarrow MH_x + \Delta H \qquad (3\text{-}1)$$

where M, x, H, and MH denote the metal or metal alloy, non-stoichiometric coefficient, hydrogen, hydride phase of the metal or metal alloy, respectively. The last term ΔH represents the enthalpy change of the reaction. Thus, the reaction rate highly depends on the heat transfer of ΔH from the metal hydride reactor.

Several research groups have reported technologies to improve the heat transfer capacity of various metal hydrides [6–10]. Most of these efforts were put towards enhancing the thermal conductivity of metal hydride powder. Metal hydride compacts that were pressed at a high

pressure were proposed [6–8]. The compacts increased the thermal conductivity of metal hydride from 0.1 ~ 2 W/m-K to 1 ~ 10 W/m-K. Ron et al. [10] and Congdon et al. [9] proposed metal hydride pellets, also known as porous metal hydride. Their techniques require sintering under high pressures and the use of an organic binder. However, both the compacts and porous metal hydrides require an additional preparation and cause a reduction in mass transfer of hydrogen due to their low permeability.

In this research, we propose extended heat transfer surface structure. Instead of increasing the thermal conductivity of the metal hydride, fins structures are employed to enhance the heat transfer of metal hydride alloys in the cylindrical reactor. Numerical simulations are performed based on a multiple-physics modeling to analyze the transient heat transfer during the hydrogen absorption process. The objective is to minimize the time elapsed for the process and to reduce the hotspot temperature by determining the number and shape of rectangular fins while the total volume of fins used are fixed. Reduction in the hotspot temperature is the secondary objective. High temperatures are the primary cause of decrepitation of metal hydride powder, which leads to the congestion of fine hydride powders. The fracture of the metal hydride can happen after hydriding-dehydriding cycles at high temperatures.

3.3 Reactor model

One of the most feasible configurations for metal hydride based hydrogen storage systems is in-line or staggered banks of reactor cylinders. The liquid coolant flows over the cylinder bank in a form of cross-flow. In such a heat transfer configuration the external convection heat transfer is very effective. Thus, the most thermal resistance is attributed to the conduction heat transfer between the metal hydride to the reactor wall.

41

Rectangular fins are applied to the inner surface of the wall of a cylindrical reactor. Figure 3.1 shows the cross-sectional view of the reactor having six fins. The reactor of 50 mm in outer diameter has 2 mm thick wall. The shape of fin is characterized by the aspect ratio, the thickness to the length. The reactor wall and the fins are one piece of solid body. The reactor has a constant cross-section along the axial direction. The metal hydride powder is filled in the space that the fins and inner surface of the wall make. In this study, LaNi$_5$, one of the most commonly used metal hydrides, is selected for numerical study.
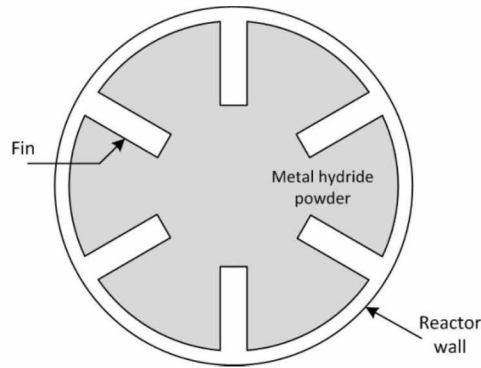
Figure 3.1: Cross-section view of 6-fin reactor

3.4 Hydriding process

The hydriding process of powder of LaNi$_5$ metal alloy can be modeled by taking into account the mass conservation of hydrogen-absorbed metal alloy, Darcy flow in the porous medium, and heat generation by exothermic reaction during the hydriding process. The mass conservation of the hydrogen-absorbed metal hydride is involved in the diffusion of hydrogen into the powder,

$$\frac{\partial c}{\partial t} = \nabla \cdot (D\nabla c) + R \tag{3-2}$$

The diffusivity of hydrogen D in LaNi$_5$ was studied by Majer [11]

$$D = D_0 \exp\left(-\frac{H_a}{k_b T}\right) \tag{3-3}$$

While the density of the solid phase is solved from the mass equation above, the pressure field in the reactor can be obtained by considering the hydrogen flow in the metal hydride powder to be a Darcy flow:

$$\varepsilon \frac{\partial \rho_g}{\partial t} = \frac{\kappa}{\mu} \nabla \cdot \left(\rho_s \nabla p\right) - \left(1 - \varepsilon\right)\dot{m} \tag{3-4}$$

The hydrogen gas density is obtained by the ideal gas law. An assumption that the gas temperature T_g remains constant at the room temperature is made for reducing computational load. Temperature distribution in the porous metal hydride is identified via the energy conservation:

$$\rho_0 c_{p_z} \frac{\partial T}{\partial t} = k_s \nabla^2 T + \left(1 - \varepsilon\right)\dot{m}\Delta H \tag{3-5}$$

The enthalpy of formation ΔH acts as the source of heat generation. The heat transfer between the metal hydride powders and the surrounding hydrogen gas is neglected. Another assumption is that the viscous dissipation and compression work due to the flow of hydrogen in the reactor bed are negligible. The mass flow rate during the absorption process is written by

$$\dot{m} = C_a \exp\left(-\frac{E_a}{RT}\right) \ln\left(\frac{p}{p_{eq}}\right)\left(\rho_{sat} - \rho_0\right) \tag{3-6}$$

The pressure at constant temperature state can be determined by the van't Hoff relationship:

$$P_{eq} = exp\left(A - \frac{B}{T}\right) \tag{3-7}$$

43

The equilibrium pressure p_{eq} in Eq. 3-7 is in the unit of atm, and the van't Hoff constants A and B are empirically determined.

Numerical computation was conducted to solve the multi-physics reaction process described by Eqs. 3-2 through 3-7 using COMSOL™, a commercial partial differential equation solver [12]. Aluminum 2024 T6 was selected for the reactor and fins material (thermal conductivity: 177 W/m-K). The thermal conductivity of LaNi$_5$ powder is set to be 2 W/m-K. The hydrogen supply pressure is set to be 6.895 bar. The coolant temperature and initial temperature of the reactor are 10°C. The convective heat transfer coefficient of the coolant that flows over the outer surface of the reactor is assumed 1,000 W/m^2-K.
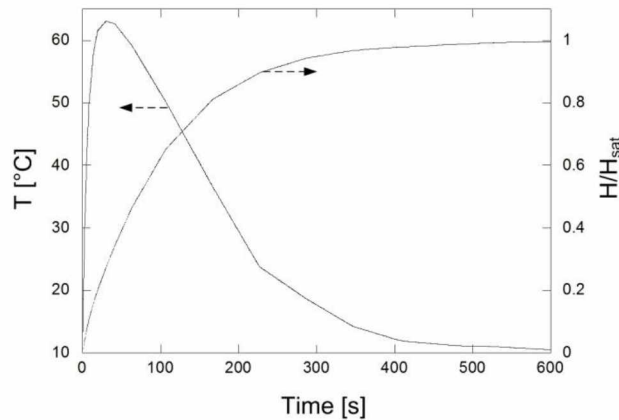
Figure 3.2: The volume-average temperature of metal hydride and hydrogen absorption over the process time.

Figure 3.2 exhibits the simulation results of the hydriding process for the case of no fins. The volume averaged temperature of metal hydride powder and ratio of the mass of absorbed hydrogen to the saturation mass are plotted in the graph. The hydriding rate is very high in the beginning and slows down. It is because of the delay caused by slow heat transfer. As a result, the temperature sharply rises for approximately the first half a minute and then gradually

decreases. More than 90% of hydrogen is absorbed within 300 seconds. With a better fin structure the time required for absorption is expected to shorten. In the next section, the optimal number and shape of fins will be sought.

3.5 Heat conduction model

The hydriding process of metal hydride reactors can be viewed as a transient heat conduction of two solid bodies having a convective boundary condition on the outer body and time-variable heat generation in the inner body. To reduce the computation time the hydriding process model described in Sec 3.4 is simplified to a transient heat conduction with a predefined time-variable heat generation. The exothermic reaction is simulated as a pulse of volumetric heat generation. Thus, the last term $(1-\varepsilon)m\Delta H$ per a unit volume is replaced by a sinusoidal function:

$$
\begin{aligned}
Heat\,Gen &= \dot{E}_{gen,peak} \sin\left(\frac{\pi t}{30}\right) && \text{for } t \le 15s \\
&= \dot{E}_{gen,peak} \sin\left(\frac{\pi(t+30)}{90}\right) && \text{for } 15s < t < 90s
\end{aligned}
\tag{3-8}
$$

The peak heat generation rate $\dot{E}_{gen,peak}$ that makes Eq. 3-8 equivalent to the actual heat generation is calculated approximately 2.0 W/cm^3.

3.6 Fin optimization

For optimization study all the conditions are the same as before except for the number of fins and their aspect ratio. In this report the volume fraction ratio remains $\varphi = 0.1$. The volume fraction is defined as the ratio of the volume occupied the fins to the total volume occupied by the metal hydride powder when no fins are attached. Therefore, the cross-sectional area of all fins must be $\varphi \pi r_i^2$, where r_i is the radius of the inner surface of wall. The optimization begins with a search for the best aspect ratio with a fixed number of fins. For example, the aspect ratio is varied from 0.138 to 0.283 for the 3 fins reactor.

COMSOL™ is used for numerical heat transfer. The number of element is more than 1,000. The time step is 0.05 seconds. The dimensional tolerance is 10^{-8} m. An example of the temperature distribution on the reactor cross-section is seen in Figure 3.3. This is a 6-fin reactor with the aspect ratio of 0.0958 (1.629 mm × 17.00 mm) 60 s after the hydriding process. It shows that the hotspot is located in the center and local hotspots form in the middle of the sliced-sector-shaped area.

To reduce the computation load, the half of sliced sector area is taken as model geometry. This is possible because symmetry lines are along the centerline of the fins and the middle angled line between two neighboring fins.
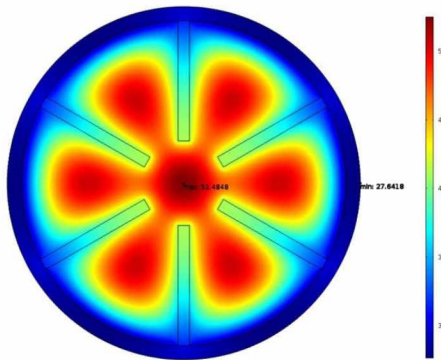
Figure 3.3: Temperature distribution of 6-fin reactor at 60s.

3.6.1 Optimization of aspect ratio

The aspect ratio, defined as the thickness of the fin relative to the length of the fin, is one of the key parameters in the design optimization. There exists an optimal aspect ratio that best suits the design, yielding the most effective cooling with a fin shape that is not too short and not too long. For an example, consider the 6-fin structure shown in Figure 3.1. By altering the fin's

46

aspect ratio the hotspot temperature and the heat transfer from the metal hydride can be improved to minimize the time elapsed to cool to 15°C and to reduce the hotspot temperature.

The results of COMSOL™ simulations for the 6-fin reactor are presented in Figure 3.4. It is clear that the optimum aspect ratio is located at the lowest point on the curves. For the time required to cool to 15°C, the optimum design is found at the aspect ratio of approximately 0.9, and the corresponding cooling time is 134 seconds. Examination of the hotspot temperature curve shows that the maximum observed hotspot temperature is at a minimum value of 62.1°C for the aspect ratio of 0.85. All other values along the curve are greater for the points plotted. From the both curves in Figure 3.4 one can see that the optimal aspect ratio stays less than 0.1 and a drastic upsurge is observed in the time taken to cool down to 15°C and the hotspot temperature when the aspect ratio is greater than 0.1. The optimum aspect ratio is therefore determined by varying the length and thickness of the fin under examination. If the fin length is too long, it is more difficult to deal with the hotspots occurring in the middle of the sliced pizza. Conversely, if the fin is too short, the insufficient fin length makes it difficult for the high conductive thermal path (the fins) to reach the hot spot at the center of the reactor.

3.6.2 Optimization of number of fin

The number of fins is an important factor in reactor design. With a fixed volume fraction at 0.1, we seek the optimal number of fins. Reactor designs with different numbers of fins (N) are numerically examined in the same fashion as Section 3.6. The optimization begins with the N = 3 design. The minimum time required to cool to 15°C and the lowest hotspot temperature are found by varying the aspect ratio as in the previous section. This optimization continues for N = 4, 6, 8, 10, 12, 18, 32, 48.
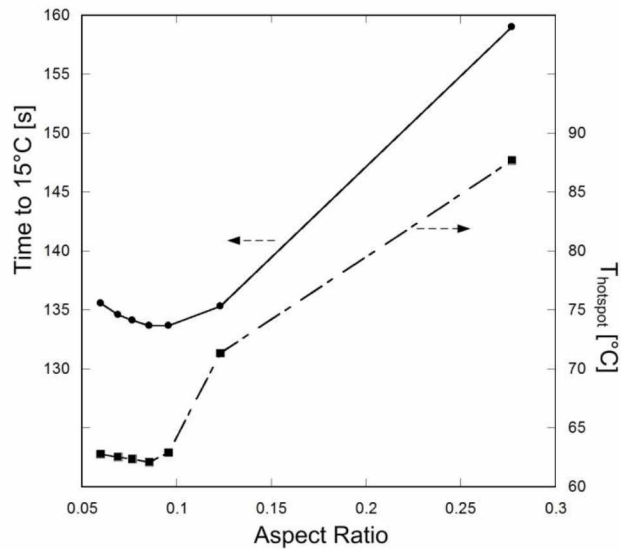
Figure 3.4: Time required to cool down to 15°C and the maximum hotspot temperature for the 6-fin reactor.

In Figure 3.5, the computed results for the minimum time required to cool down to 15°C and lowest hotspot temperature are displayed. The reactor model performs better with an increase in the number of fins. From this simulation data, it is observed that the required time to cool for the 3-fin design is 153.9 seconds. This value decreases to 122.7 seconds for 48-fin design. The hotspot temperature also decreases with more fins. However, increasing the number of fins adds complexity to the reactor model, which can be detrimental from the point of view of construction and assembly.
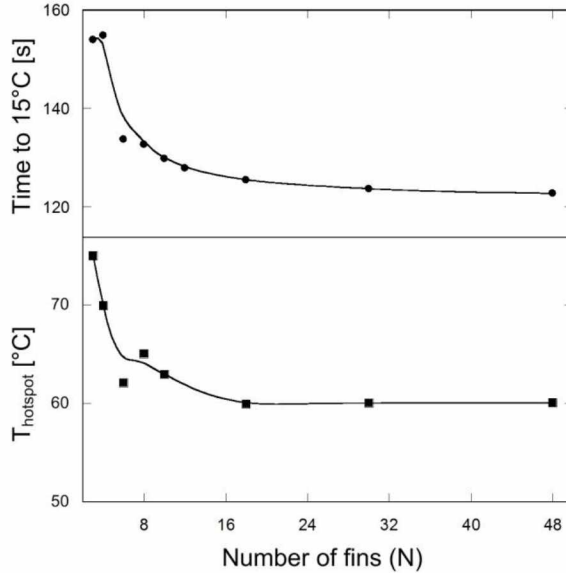
Figure 3.5: Optimum number of fins for minimum time to cool to15°C and lowest hotspot temperature.

For $N = 16$ or more, any reasonable benefit in increasing the number of fins are no longer expected as no further time saving and drop in hotspot temperatures is observed. Many fins yield a very complex internal design structure.

3.7 New construct

A new design is developed to enhance the performance of the reactor model even further. In this design, two sets of fins are modeled: short fins and other long fins are placed adjacent to each other. The length of long fins doubles that of short fins. An example of 12-fin reactor (6 long fins and 6 short fins) is shown in Figure 3.6. In Case A, the fins are modeled with the fin thickness ratio of 1:1, where both the long and short fins have the same thickness. Again, the volume fraction remains 0.1 for a fair comparison with the previous one-level designs. Computational study is performed with varying the aspect ratio for the time required to cool down to 15°C and minimum hotspot temperature. In Figure 3.7, the sliced-pizza shape, which is cut along the symmetry lines, is representative of a sector of the reactor with half of a long fin at the top and half of a short fin at the bottom, with the interstitial area comprised of the metal

49

hydride metal powder. The figure shows the temperature distribution of two level 12-fin reactor at 60 seconds.

Case B design has different fin thickness between long and short fins. The fin thickness ratio of Case B is 2:3. Thus, the thickness of the long fins are 1.5 times that of the short fins. In Case B as well as Case A, the long fins are twice as long as the short fins. In the present study we conducted an optimization for two-level 12-fin (6 long and 6 short fins) reactor.
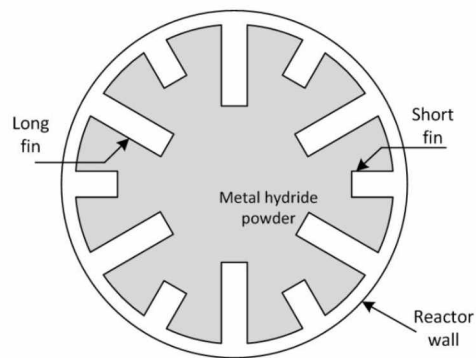
Figure 3.6: Two level fin design with 6 long and 6 short fins.
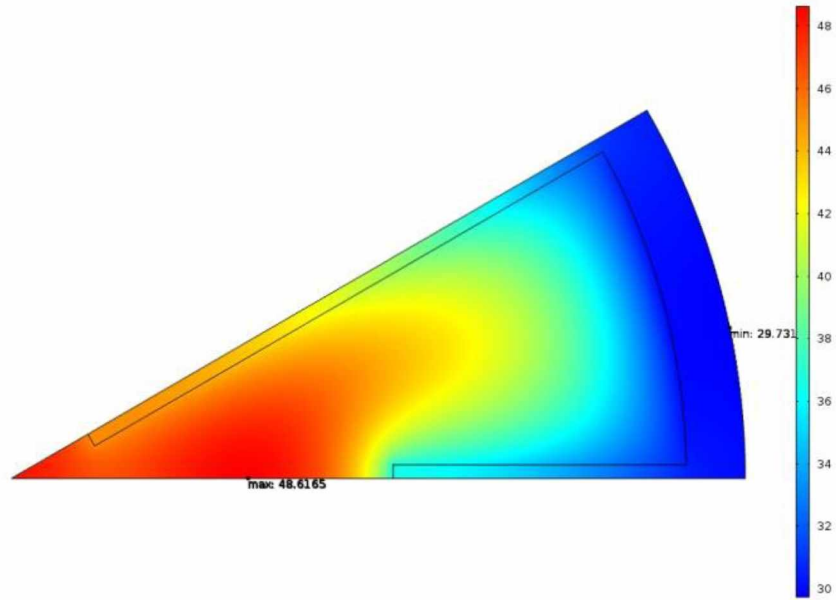
Figure 3.7: Temperature distribution on two-level 12-fin reactor.

Simulations reveal that both cases have an optimum aspect ratio for the same reason as in the single level fin reactors. Too long fins (low aspect ratio designs) are ineffective for the hotspot located in the middle of the sliced-pizza area while too short fins (high aspect ratio designs) are vulnerable to hotspots in the center of the circular reactor. Results for the Cases A and B in comparison with single level are summarized in Table 3.1.

Table 1.1: Two-level 12-fin reactors vs single-level reactor.

Case	Optimal aspect ratio	Time to 15°C [s]	$T_{hotspot}$ [°C]
A	0.0462	129.1	57.97
B	0.0546	128.9	57.47
single level 6-fin	0.0855	133.7	62.09

Case A yields an optimum aspect ratio taking 129.1 seconds to reach 15°C and a maximum hotspot temperature of 57.97°C. With Case B, both the time to cool to 15°C and minimum hotspot temperature are lower at 128.9 seconds and 57.47°C, respectively. It can be inferred that Case B exhibits slightly improved performance in these respects. When the two level fins designs are compared to the single level 6-fin case, Cases A and B outperforms the single level reactor for both time elapsed to 15°C minimum hotspot temperature. The hotspot temperatures for two level designs are more than 4 K lower than for single level design. Therefore, the new construct provides a highly effective way to transport heat to outside environment from the confined volume.

3.8 Concluding remarks

In this paper, we reported a numerical study on design optimization of the metal hydride reactors for hydrogen energy storage. The simulation study revealed the optimum aspect ratios of rectangular fins for accelerating heat rejection and lowering the hotspot temperature in a cylindrical metal hydride reactor. The objectives were met: (i) optimal aspect ratio of the fins was determined and (ii) optimum number of fins for heat transfer performance as well as ease in manufacturing was suggested. If design complexity is not a factor to consider, a design with many fins are recommended.

In addition, a new construct design was proposed: two level fins with long and short fins. The long fins dealt with the hotspot in the center of the reactor while the short ones with the local hotspot positioned in between two neighboring long fins. The relationship between total number of fins and time to reach 15°C is summarized by the following observations: (i) the original 6-fin case shows that 133.7 seconds are needed to reach 15°C. The maximum hotspot temperature at this point is observed to be 62.08°C. (ii) Case A design shows that 129.13

seconds are needed to reach 15°C. This corresponds to a thickness ratio of 1:1 and a maximum hotspot temperature of 58.26°C. (iii) Case B design improves upon the previous, with 128.92 seconds to reach 15°C, corresponding with a maximum hotspot temperature of 57.47°C for the optimum 2:3 thickness ratio.

3.9 Nomenclature

c	concentration of the hydrogen, mol m^{-3}
C_p	specific heat, J kg^{-1} K^{-1}
C_a	constant
R	reaction rate, mol m^{-3} s^{-1}
H_a	activation enthalpy, eV
k	thermal conductivity, W m^{-1} K^{-1}
k_b	Boltzmann constant, eV K^{-1}
ε	porosity
ρ	density, kg m^{-3}
κ	permeability, m^2
μ	viscosity of hydrogen, Pa s

subscripts

0	initial state
eq	equilibrium
g	hydrogen gas
s	metal hydride powder

3.10 References

1.   C. Corgnale, B.J. Hardy, D.A. Tamburello, S.L. Garrison, D.L. Anton. Int. J. Hydrogen Energy, 37,3, pp. 2812–2824 (2012).

2.   S.N. Nyamsi, F. Yang, and Z. Zhang. Int. J. Hydrogen Energy, 37, 21 pp. 16078–16092 (2012)

3.   A. Souahlia, H. Dhaou., F. Askri, M. Sofiene, A. Jemni, S. Ben Nasrallah. Int. J. Hydrogen Energy, 36, 20, pp. 12918–12922 (2011)

4.   A. Souahlia, H. Dhaou, S. Mellouli, F. Askri, A. Jemni, S. Ben Nasrallah. Int. J. Hydrogen Energy, 39, 14, , pp. 7365–7372 (2014)

5.   S.L. Garrison, B. J. Hardy, M. B. Gorbounov, D. a. Tamburello, C. Corgnale, B. a. Vanhassel, D. a. Mosher, D. L. Anton. Int. J. Hydrogen Energy, 37, 3, pp. 2850–2861 (2012)

6.   M. Dieterich, C. Pohlmann, I. Bürger, M.Linder, L. Röntzsch. Int. J. Hydrogen Energy, 0, 711, pp. 6–13 (2015)

7.   K. J. Kim, B. Montoya, A. Razani, K.H. Lee. Int. J. Hydrogen Energy, 26, 6, pp. 609–613 (2001)

8.   H. P. Klein, M. Groll. Int. J. Hydrogen Energy, 29, 14 , pp. 1503–1511 (2004)

9.   Congdon, W. , US patent, 5443616 (1995)

10.   M. Ron, E. Bershadsky. J. International Journal of Hydrogen Energy, 17 (1992)

11.   G. Majer, U. Kaess, R. B. J., Physical review B, 57 (1998).

12.   http://www.comsol.com/ for more information about COMSOL multiphysics (2015).

Chapter 4

Optimization of Internal Cooling Fins for Metal Hydride Reactors

4.1 Abstract

With the worldwide need to reduce the emissions from fossil fuel use, hydrogen is being considered as a possible future fuel. Hydrogen, as a clean energy carrier, needs to be stored and pressurized to increase the energy density to allow for economical transportation and use. However, the traditional way to pressurize and store hydrogen requires a significant amount of compression power as well as large size of container. Metal hydride alloys are considered as a promising alternative to conventional hydrogen storage cylinders and mechanical hydrogen compressors. Compared to storing in a classic gas tank, metal hydride alloys can store hydrogen at nearly room pressure and use less volume to store the same amount of hydrogen. However, this hydrogen storage method necessitates an effective way to reject the heat released from the exothermic hydriding reaction. In this paper, finned surface is adopted to improve the heat rejection in the cylindrical reactor. The fins collects the heat that is volumetrically generated in $LaNi_5$ metal hydride alloys and deliver it to the channel located the center, through which a refrigerant flows. The heat transfer is accomplished by the vaporization of the refrigerant. Numerical simulations are performed based on a multiple-physics modeling to analyze the transient heat transfer during the hydrogen absorption process. The volume-averaged temperature of the reactor is plotted over the time elapsed for the process. Fin design is made to identify the optimum shape for the best heat transfer.

4.2   Introduction

In Alaska, interior villages majorly rely on conventional heating power for daily requirements, such as those from combustion-based generators, which use diesel or gasoline as fuels [1]. However, the residents who depend on these fuels are greatly affected by the increasing costs of imported fuels, which are used in heating, electricity generation and transportation. This negative effect to consumers can be mitigated as Alaska possesses large quantities of renewable energy (RE) resources; wind, geothermal, tidal etc. However, specific applications for each technique must be location-specific to areas, which would support their use. For example, along the coastal regions of Alaska such as Barrow, Nome, Wales, Homer and similar locations, the annual windfall is much greater than that received by towns and villages in the interior of the state. Therefore transportation of any renewable energy gathered from these sites to locations in the interior villages is much more difficult from the technical and maintenances point of view. Taking this situation into consideration, also noting that remote villages regularly will pay a higher economic and environmental penalty for their energy generation [2], the proposal to implement energy storage technologies such as the metal hydride reactor with rapid hydrogen absorption is a very lucrative pursuit. This increased penalty is due to the additional effort required to transport any fuel to remote interior regions, including the environmental hazards of storing this fuel which can sometimes result in damaged or leaking fuel tanks, discarded drums and containers, and the like. It is this fact, which makes RE technologies so lucrative to rural consumers in Alaska. If rural customers are given the capability to generate and store their own local energy supply, this reduces the need for importing fuel transportation into the region, and also optimizes the life-cycle cost for a localized integrated energy system. Effective energy-storage methods offer the capability to increase the energy storage periods up to more than a

56

week in many cases, with even longer-term storage solutions available, specifically when using metal hydride reactor systems to increase the level of efficiency when using hydrogen as a fuel source [3–13].

The benefits of using hydrogen as a fuel source traditionally come with added risks: as a gas, hydrogen can be extremely flammable, it requires high energy in order to compress and store in a holding vessel. The metal hydride reactor system eliminates much of these concerns: firstly, the metal hydride powder ($LaNi_5$) more efficiently stores hydrogen atoms within its molecular structure versus hydrogen freely stored in the gaseous state, owning to the high uptake capacity. Second, the volume space required for each storage vessel is much smaller when the lanthanum nickel powder is used, saving material, assembly, and fabrication costs and on-site storage space. The pressure at which hydrogen can be stored is significantly lower when using metal hydrides, typically a similar amount of hydrogen can be stored at nearly room pressure. A third benefit is that the metal hydride renders the hydrogen in a less volatile state, making transportation much safer, further reducing transportation cost to the end consumers.

Introducing the concept of metal hydrides begins with defining their composition: which is a combination of hydrogen and a metal or metal alloy. Via surface chemisorption, these hydrides can absorb a large relative amount of hydrogen per unit weight. It is this inherent large hydrogen update capacity which is the most appealing aspect of the technology for use in energy storage versus conventional H_2 storage methods [14–16] . As mentioned, traditional H_2 storage necessitates high pressures, while metal hydride alloys store the same amount of H_2 at nearly room pressure. However, H_2 absorption does necessitate an effective way to reject the heat released from the exothermic reversible hydriding reaction.

$$M + \frac{x}{2}H_2 \leftrightarrow MH_x + \Delta H \qquad\qquad (4\text{-}1)$$

Note that M, x, H and MH denotes the metal or metal alloy, non-stoichiometric coefficient, hydrogen, and hydride phase of the metal or metal alloy, respectively. The ΔH term represents the change in enthalpy. As this reaction chemically generates a considerable amount of heat, a method for efficiently rejecting this from the metal hydride reactor is critical to effective system implementation. The hydride powder itself possesses a low thermal conductivity value, and to this end various research groups have developed methods to improve heat transfer capacity of the material. From efforts to enhance the inherent thermal conductivity of the metal hydride powder [17–22], to metal compacts pressed at high pressure [17], to pellet-shaped geometries known as porous metal hydride [19], all of these advances require sintering under high pressure and the use of an organic binder.

Also, within this paper the implementation of the constructal architecture will be used in optimizing the heat transfer performance in favor of increasing hydrogen absorption. The constructal law accounts to the flow systems observed in nature, with the design evolving freely in time in order to facilitate access to the currents flowing through it. Furthermore, the system evolves in such a way that it provides easier accesses to the currents in order to overcome flow resistances over space and time, thereby generating highly efficient global flow configurations. Applications of this theory are widespread and include the domains of heat transfer [23–25], Geology [26,27] as well as Biology [28]. The motivation behind constructal theory takes into account reduction (optimization) of the overall complexity, such that new constructs allow the structure to improve overall heat transfer performance.

In this paper, high-conductive finned surface is adopted as the main method to improve the heat rejection from $LaNi_5$ metal hydride alloys in two specific cases. First, a refrigerant flows

through channels inside the cylindrical metal hydride reactor combined with the increased thermal cooling area provided by internally located fins. The second case also uses internally located fins along with external outside convection for increased thermal cooling. These two cases are analyzed and compared based on overall cooling performance of the reactor model. To this end, numerical simulations are used based on multi-physics modeling with the goal of analyzing transient heat transfer during the H_2 absorption process. The goal being to minimize the elapsed time for the process via determination of the number and shape of rectangular fins while the total volume of fins used remains fixed. Reduction of the hotspot temperatures is the secondary objective, as high temperatures are the primary cause of decrepitation of metal hydride powder, which can lead to congestion of finer hydride powders. The fracture of the metal hydrides can occur after hydriding-dehydriding cycles running at high temperatures.

4.3   Metal Hydride Reactor Model

In one example of this design, hydrogen is supplied to the cylindrical reactor, which is 100 mm in diameter, and flows through the metal hydride powder along the length of the reactor cylinder as shown in Figure 4.1. In this study, $LaNi_5$ is selected for metal hydride powder. The refrigerant flows in a 12 mm diameter coolant channel (the central tube) in the axial direction. The reactor cylinder employs a series of internally mounted rectangular fins, which act as increased cooling surface area to absorb the heat generated from the exothermic hydriding reaction to the refrigerant. These fins are mounted from the exterior surface of the central tube and extend radially outward at predetermined lengths and aspect ratios. This configuration lends to cooling via conduction heat transfer from the metal hydride powder within the reactor to the central tube, and then the heat is rejected as the refrigerant changes its phase from liquid to vapor. A second iteration of the in-line cylinder design incorporates all of the attributes of the

previous example, and further enhances the thermal cooling effect by taking into account the external convection from the environment around the reactor cylinder. The environment in this case is analyzed at a value of 500 W/m²-K for the convective heat transfer coefficient of cooling water, which is a generally accepted mean value for this medium.
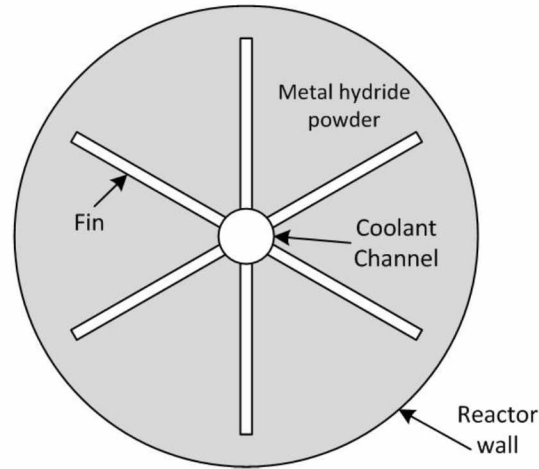
Figure 4.1: Six-fin reactor model with the central cooling.

Considering the fin design in the reactor model we follow a constructal approach to acquire the optimal design. A general consideration based on the assessment of some ratios between the dimensions of the system a final configuration is obtained which optimizes the required variable, following the maximization criteria. Here in this paper, we try to find the optimal aspect ratio, defined as the thickness of the fin relative to the length of the fin, which best suites in achieving reduced hotspot temperature and favors hydrogen absorption process.

4.4   Hydriding process

Based on the processes of heat generation via exothermic reactions for the chemical hydriding process, along with flow in porous mediums, and also considering the mass conservation of hydrogen-absorbed metal, the full description of the LaNi₅ metal alloy can be accurately modeled, and it is exactly this procedure which is described in the proceeding section.

Beginning with the mass conservation of the hydrogen-absorbed metal hydride as the diffusion of hydrogen occurs into the LaNi$_5$ powder:

$$\frac{\partial c}{\partial t} = \nabla \cdot (D\nabla c) + R \tag{4-2}$$

Considering that the diffusivity of hydrogen, D, in LaNi$_5$ as referenced by [29]

$$D = D_0 exp\left(-\frac{H_a}{k_b T}\right) \tag{4-3}$$

The density of the LaNi$_5$ metal hydride powder increases as it absorbs hydrogen and thus it is solved from the preceding mass equation. The temperature distribution in the metal hydride powder is identified by the energy conservation equation:

$$\rho_0 c_p \frac{\partial T}{\partial t} = k_m \nabla^2 T + (1 - \epsilon)\dot{m}\Delta H \tag{4-4}$$

Examination of the heat generation identifies the enthalpy of formation, ΔH, to be the source of the temperature increase. At this point two assumptions are made: one, which gas temperature Tg remains constant at room temperature to assist with computational processing load, and two, that the hydrogen gas density as obtained from the ideal gas law is valid for further calculations. Further simplification neglects the effects of heat transfer between metal hydride powders and surrounding hydrogen gas. Furthermore, it can be assumed that the viscous dissipation and compression work due to the H$_2$ in the reactor bed are negligible. For the absorption process, the mass flow rate is described by:

$$\dot{m} = C_a exp\left(-\frac{E_a}{RT}\right) ln\left(\frac{P_{in}}{P_{eq}}\right)(\rho_{sat} - \rho_0) \tag{4-5}$$

Incorporation of Van't Hoff's relationship for pressure at constant temperature states is also given by the proceeding equation, with equilibrium pressure p_{eq} in units of atm, and the contstants A and B being empirically determined.

$$P_{eq} = exp\left(A - \frac{B}{T}\right)$$ (4-6)

COMSOL™, a commercial partial differential equation solver [30] was used to evaluate numerical computations to solve multiple physics reaction processes as described from Eqs.4- 2 through 4-6. For the fin material, aluminum 2024 T6 (thermal conductivity: 177 W/m-K) was selected, while the thermal conductivity of LaNi$_5$ powder was set to a value of 2 W/m-K, and the H$_2$ supply pressure valued at 1.013 MPa. The refrigerant which runs through the center-flow tube was assumed to change its phase at a saturation temperature at 10°C. Initial temperature is also set at 10°C for the metal hydride powder and the fins.

Figure 4.2 below describes the simulation results of the hydriding process for the case of 8 fins without the additionally added external convection on the outer surface of the reactor wall. The volume averaged temperature of metal hydride powder and ratio of mass of absorbed H$_2$ to the saturation mass (H/H$_{sat}$) are plotted in the left and right ordinates, respectively.
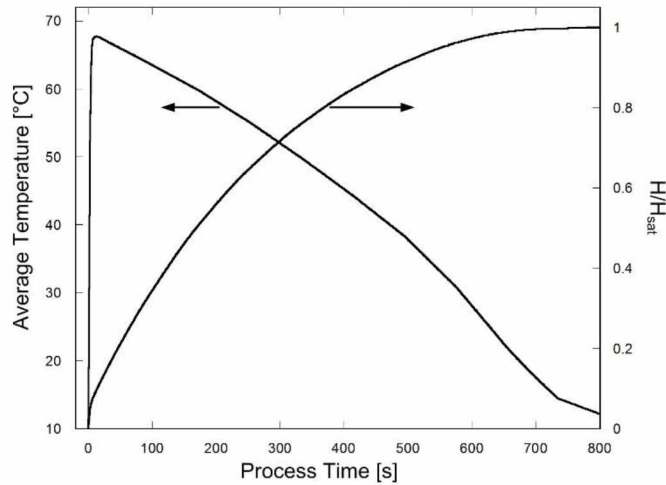
Figure 4.2: The volume-average temperature of metal hydride and hydrogen absorption over the process time.

It is observed that the hydriding rate begins at a high value and then slows, which is due to the delay caused by slow heat transfer. Thus, a resulting increase in temperature occurs for the first 15 seconds, after which this too exhibits a gradual decrease in time. At least 90% of the H_2 is absorbed within 500 seconds. It can be deduced that improved fin structure can contribute to decreased time required for absorption overall. The optimal shape of the fins is further discussed in detail in the following section.

4.5   Heat generation model

The hydriding process for metal hydride reactors can be described as follows: in the boundary between the central refrigerant channel and the interstitial metal hydride powder, the dirichlet boundary condition is included. Considering the Dirichlet boundary condition is valid for this model because heat transfer coefficient of the evaporation is of very high value so that the temperature of the surface can be viewed as a constant value with negligible error.

In an effort to reduce the computational processing time, the hydriding process model described in Section 4.4 is simplified to transient heat conduction with predefined time-variable heat generation properties, and exothermic reactions are simulated as pulse-frequency volumetric

heat generation. The last term $(1 - \epsilon)\dot{m}\Delta H$ per a unit volume in Eq. 4-4 is therefore replaced by a sinusoidal function:

$$Heat\ Gen. = \dot{E}_{gen,peak} \sin\left(\frac{\pi t}{30}\right) \quad \text{for } t \le 15\text{ s}$$

$$\text{(4-7)}$$

$$Heat\ Gen. = \dot{E}_{gen,peak} \sin\left(\frac{\pi(t + 30)}{90}\right) \quad \text{for } 15\text{ s} < t \le 90\text{ s}$$

A peak heat generation rate, $\dot{E}_{gen,peak}$ of 5.0 W/cm^3 makes Eq. 4-7 equivalent to the actual calculated heat generation value, and thus it is used for the rest of simulations.

4.6   Fin optimization

The optimization incorporates the study of all the design conditions described in the previous sections, taking into consideration specifically the number of fins and their aspect ratio. This report maintains a volume fraction of φ = 0.1 in the calculations, which is defined as the volume occupied by the fins over the total volume occupied by the metal hydride powder if no fins are present. As such, the cross sectional area of all fins is defined by , where r1 and r2 are the outer radius of the cooling tube and the inner radius of the reactor wall, respectively. The optimization begins with determination of the most suitable aspect ratio with a fixed number of fins. Here, the COMSOL multi-physics simulation software is used to calculate the transition heat transfer numerically with a model using more than 1,000 individual elements, a time step of 0.1 seconds, and a dimensional tolerance of 10-8 m. An example of the thermal distribution on the reactor cross-section is displayed in Figure 4.3 below. This 8-fin reactor has an aspect ratio (AR) of 0.06048 (2.419 mm x 40.00 mm). Figure 4.3, which exhibits temperatures 60 seconds after the hydriding process, illustrates that the minimum temperature is located at the center of the cooling cylinder, while the maximum temperature is at the inner surface of the reactor wall. In order to minimize the computational load for the simulation, only half of the fin geometry is

analyzed below. As the fin is symmetrical about the longitudinal axis, this is a sound practice and is considered acceptable.
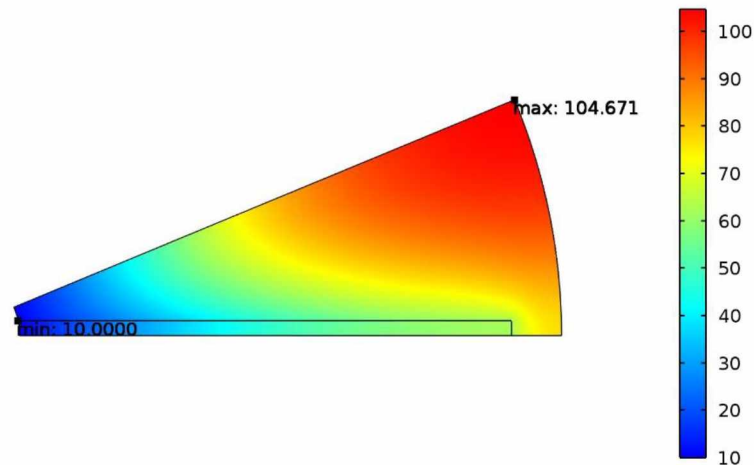
Figure 4.3: Temperature distribution of 8-fin reactor at 60s.

If fin number optimization is not carried out, the consequences can include localized hotspots due to the effect of higher temperatures in the metal hydride powder. If the metal hydride powder is allowed to collect at a location and not evenly distributed, this can result in a localized hotspot with temperatures in excess of what would be seen otherwise. This in turn can result in lowered reactor material strength due to overheating, which may result in shorter material lifespan/failure.

4.7   Optimization of aspect ratio

One of the key parameters in the optimization of the design is that of the aspect ratio (AR), which is defined as the fin thickness relative to the fin length. Within the realm of possible values for the parameter, there exists an optimal AR, which best applies to the design and therefore yields the most effective cooling with a fin geometry that is neither too long nor too short. As an example, referencing the 8-fin design in Figure 4.3, the fin's aspect ratio can be altered to yield a beneficial result of dispersing thermal hotspots and improving the heat transfer

away from the metal hydride powder towards the fins themselves. Furthermore, the time required for cooling can be minimized to achieve the desired 15°C at any given thermal hotspot. To this end, Figure 4.4 shows a plot of the average temperature versus the elapsed time for two distinct fin AR's. The cooling time required, for example to achieve 30°C, exhibits a large time difference (approximately 210 seconds for 0.0605 aspect ratio versus 300 seconds for 0.1075 aspect ratio). The difference in cooling time therefore contributes to improved hydrogen absorption from the metal hydride hydriding process.

The results of the COMSOL simulation on the 8-fin design are plotted in Figures 4.5 (a), (b), where it is clear to see that the optimal aspect ratio is located at the lowest region of the parabolic curve. For example, in the Figure 4.5 (a) graph, the time needed to achieve cooling to 15°C, the optimum design is found at an aspect ratio of approximately 0.06, with a corresponding cooling time of 397 seconds. An examination of the hotspot temperature curve shown in Figure 4.5 (b) illustrates that the observed hotspot temperature has a minimum value of 105.4°C for the aspect ratio 0.05, compared with the maximum value of 108.7°C at an aspect ratio of 0.1075. This range of values between minimum and maximum temperatures illustrates that a difference of 3.3°C can be achieved with simple modifications to fin geometry.
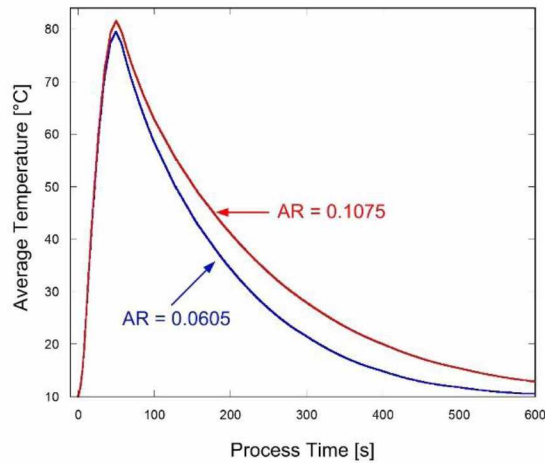
Figure 4.4: The average temperature of the metal hydride for the aspect ratio of 0.0605 and 0.1075

From the curve plots in Figures 4.5(a) and (b), it can be clearly observed that the optimal aspect ratio exists below 0.07 and that a dramatic increase in time exists in the time required to cool down to 15°C along with the associated hotspot temperatures when this aspect ratio is greater than 0.08. Therefore, the optimum aspect ratio is determined by variation of the fin length and thickness to values, which yield maximum efficacy. If optimization is not carried out, for example a fin designed too long, this can result in increased hotspot activity along the outer radius of the interior of the reactor. Alternatively, if a fin length is designed too short, the thermal transport phenomenon is much more difficult to cool any existing hotspots occurring along the outer radius of the interior of the reactor.
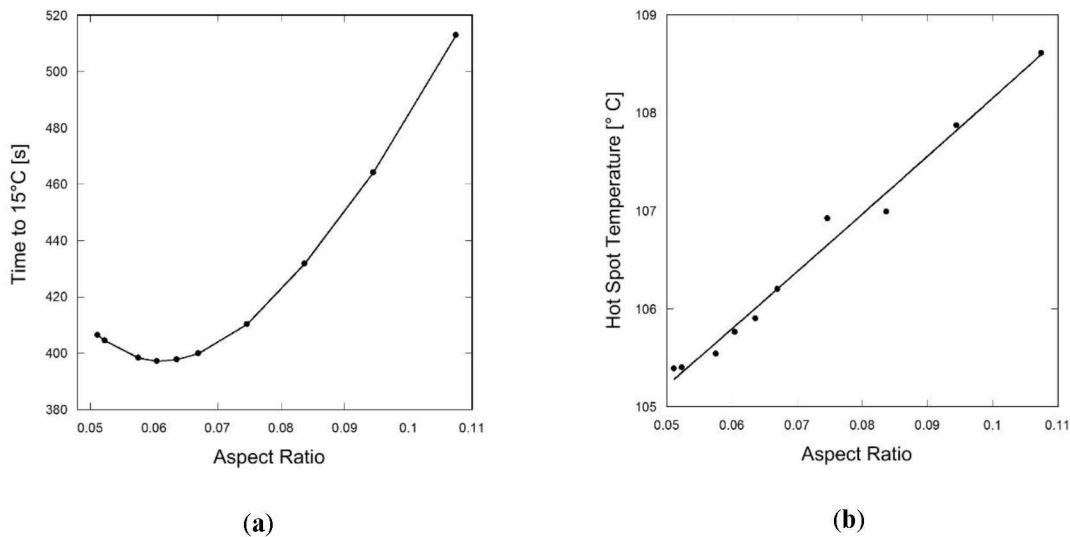
Figure 4.5: The results of simulations for the eight-fin reactor. (a) Time required to cool to 15°C, (b) Hot spot temperature.

4.7.1 Optimization of number of fins

The number of fins used is a critical factor in reactor design. Noting that a fixed volume fraction is given at 0.1, the optimal number of fins is desired from this value. Reactor designs with different fin numbers (N) have been examined numerically in a method similar to that, which is described in Section 4.7. This optimization process begins with the N=3 fin design. Here, the minimum time required to cool to 15°C and the lowest hotspot temperature are found by varying the aspect ratio via the procedure described in the previous section. Continuation of this procedure includes subsequent values of N = 4, 5, 6, 8, 12, 18, 36 and 72 fins.

In Figures 4.6 (a) and (b), the results from COMSOL simulation show the minimum time required to cool down to 15°C as well as the lowest hotspot temperature. As is seen, the reactor model shows improved performance with an increased number of fins. Viewing this simulation data, one can view that the cooling time required for the 3-fin design is 957 seconds, which can be compared to the 8-fin design, which requires 397 seconds. This trend of a decrease in the required time to reach 15°C continues asymptotically towards the 72-fin design. Additionally the

hotspot temperature decreases with increasing number of fins, however this also adds to the overall complexity of the reactor model, which can be detrimental to the construction, assembly, and maintenance of the model.
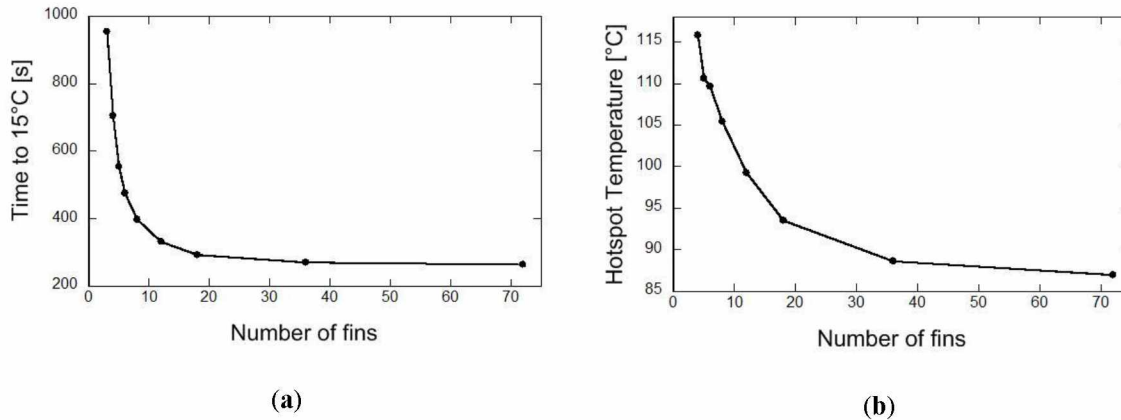
Figure 4.6: The effect of the number of fins on the heat transfer. (a) Time required to cool to 15°C, (b) Hot spot temperature.

When considering the balancing effects of model complexity to cooling efficiency, there is no longer any reasonable benefit to increasing the total number of fins after N = 18. At this point, an increased cooling with additional numbers of fins does not offset the cost of increased model complexity, nor does neither any appreciable hydrogen absorption process time nor a drop in hotspot temperature exist either. Again, many fins will contribute to an increased internal complex design structure.

4.8   External convective cooling

A new design is developed to further enhance the cooling performance of the reactor model in which one set of cooling fins are modeled plus the effect of center cooling from the refrigerant circulating within the reactor, and in addition the effect of external convection cooling from outside the reactor is analyzed. Here again, the volume fraction remains at $\varphi = 0.1$, as in the previous simulations. Computational analysis is accomplished by varying the aspect ratio for the

69

time required to cool to 15°C along with minimum hotspot temperature. In Figure 4.7 below, the "sliced pizza" shape, which is cut along symmetric geometrical lines, is representative of a sector of the reactor with half of one fin shown, and the interstitial area composed of the metal hydride metal powder. Furthermore, the effect of convective cooling from the external environment is taken into account here, which is defined at 500 W/m^2-K.
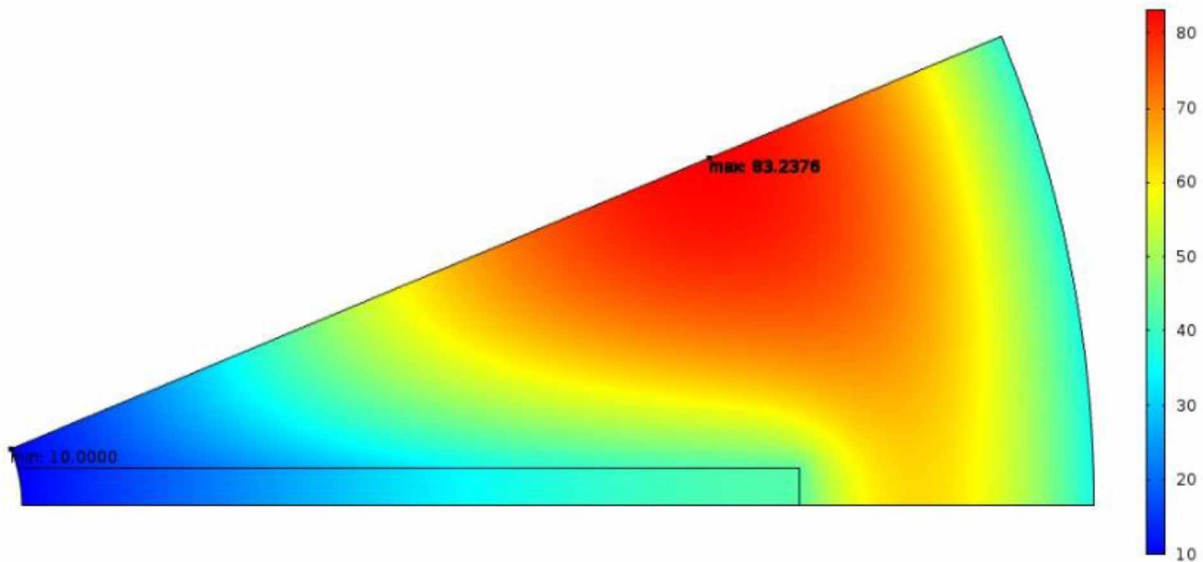
Figure 4.7: Temperature distribution of eight-fin reactor for the case of convection at 60s.

Observation of Figure 4.7 shows the majority of hotspot activity occurs within the interstitial area between the fin area and the outer radius of the interior of the reactor. In this region, the maximum observed temperature occurs at 83.24°C at a time of 60 seconds during the simulation. In comparison to the previous Figure 4.3 from Section 4.6, it is plain to see that this in an improvement as the maximum observed temperature is lower (approximately by 21°C), and also the physical location of this maximum temperature is located further into the reactor chamber, rather than just at the reactor model outer radius. Another improvement of this model from the previous is the overall thermal distribution of the hotspot maximum temperature within

the reactor. As previously stated, any localized masses of metal hydride powder will generate increased thermal resistance which can result in increased hotspot activity and can subsequently lead to detrimental material side-effects such as early fatigue. Figure 4.9 mitigates this unwanted effect via implementation of fins and the resulting thermal pattern in more evenly distributed.

The simulation reveals that an optimum aspect ratio exists for the same reasons as described in Section 4.7.1 and that fins which are too long (low AR) will be ineffective for cooling the hotspot located in the center of the sliced-pizza area, whereas fins which are too short (high aspect ratio) will be vulnerable to hotspots in the center of the reactor. Figure 4.8 below illustrates this concept further in the capacity of time required to cool to 15°C for the 8-fin reactor model.
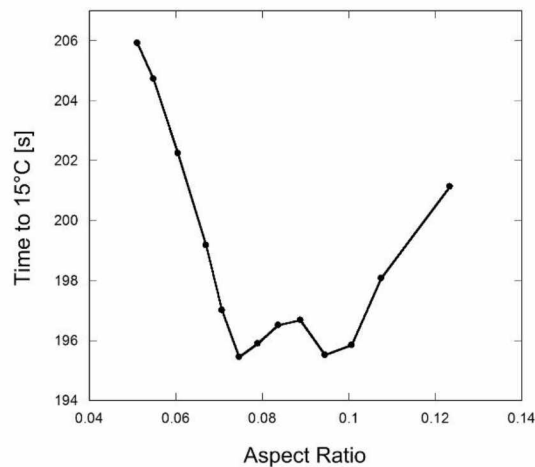
Figure 4.8: The time required to cool down to 15°C for 8-fin reactor with convection on the reactor cylinder wall

In Figure 4.8, an interesting behavior exists where two optimum aspect ratios produce the same amount of required time to reach 15°C in cooling. At 0.075 and 0.094 aspect ratios, shown at the two-pronged base of Figure 4.8, the cooling time is nearly equivalent at 195 seconds. From a design perspective this is advantageous during physical construction and assembly, as two options are available, both of which achieve maximum cooling effects. This trait offers more

flexibility via engineering design. The mechanics of why these two optimum points exist is explained as follows: (i) in the case of the 0.094 aspect ratio, which is for a shorter-length fin, the local hotspot occurs adjacent to outer edge of the fin. Here, the thermal energy is transferred from the hotspot to the fin via convection, then through the fin material via conduction, finally to the central cooling core where the refrigerant flows. (ii) in the case of the 0.074 aspect ratio, which is for a longer-length fin, the local hotspot also occurs adjacent to the outer edge of the fin. In this case, the thermal energy is removed from the system via the external convection cooling from outside the reactor. The two cases and their respective cooling effects contribute equally and thus their time required to reach 15°C is approximately the same. This coincidence may change for different situations and models when considering alternate geometry, materials, fluid coefficients, and refrigerants.

When considering the optimum number of fins to reach 15°C during cooling, this simulation analyzes the procedure in a similar method to what was described in Section 4.7.1 above. Figure 4.9 (a) illustrates the results of this analysis, which yields a cooling performance curve similar to that of Figure 4.6 (a). The number of fins analyzed for this simulation are N = 3, 4, 5, 6, 8, 12, 18, 36 and 72 fins.

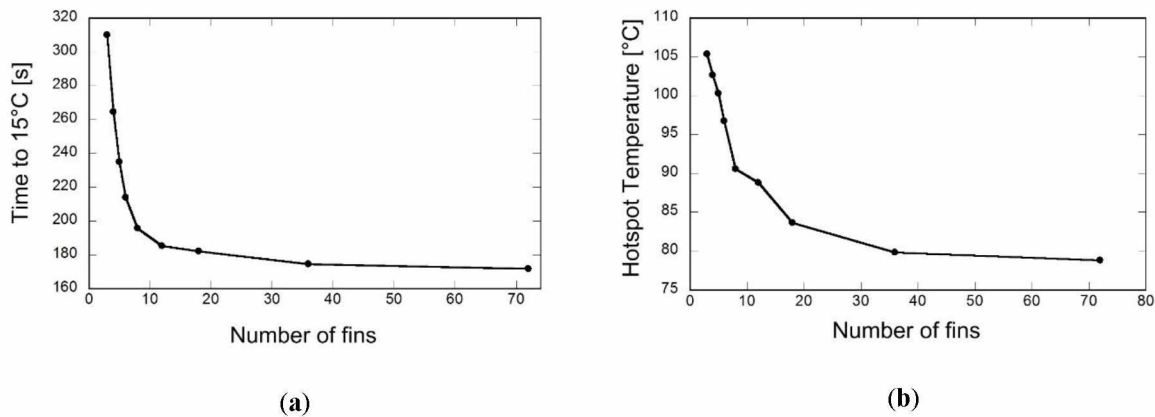(a)   (b)

Figure 4.9: The effect of the number of fins on the reactor with cooling from the external wall as well as the central channel. (a) Time required to cool to 15°C, (b) Hot spot temperature.

Here again, it is clear to note that there is a maximum cooling performance-to-cost value for total number of fins at N = 18 fins. Once again, an increase in the number of fins from this value will lead to increased complexity of the reactor model without any significant thermal cooling performance. Furthermore, it can be validated that if N = 18 fins, there is a high degree of cooling being performed within the reactor, and much improved than if N<18 fins.

The hotspot locations and temperatures are also of critical concern in the analysis, and this is considered in Figure 4.9 (b) where optimization of the number of fins, as previously discussed, yields a plot curve similar to that, which was developed in Section 4.7.1, Figure 4.6 (b). Note that once again, the numbers of fins are N = 3, 4, 5, 6, 8, 12, 18, 36 and 72.

Here, it is seen that for N = 8 the observed hotspot temperature is approximately 90°C, which is an improvement from the model in Figure 4.9 (b), where for the same number of fins, the observed hotspot temperature is 105.4°C, the hotspot temperature for the new construct convective cooling design is approximately by 15.4°C lower by comparison. This increased cooling performance can be attributed, in part, to the addition of the effect of external convective cooling from the exterior environment, with all other factors being held equivalent in the two models.

4.9   Conclusions

This paper showed that the hydriding process time to cool to 15°C and hot spot temperature reduction could be improved simultaneously by the optimal aspect ratio of the fin. The volume fraction ratio was fixed to 0.1. We explored the merits of the hydriding process time in two cases, where case (i) cooling with refrigerant circulating inside a pipe at the center of the reactor with fins and case (ii) it includes the similar conditions in the previous case along with

external convective cooling from outside of the hydrogen reactor. The simulation study revealed that the optimal aspect ratio of the rectangular fins enhances the hydration process time to cool and diminishes the hotspot temperature in a cylindrical metal hydride reactor. The optimal aspect ratios of the fins were determined and optimum numbers of fins for improved heat transfer performance were suggested to avoid overly complex structure and manufacturing process time. If the design complexity and the manufacturing process is not a factor to consider, a design with high number of fins (N=36 fins) is recommended.

Furthermore, a new construct design was proposed: considering the fin structure along with central cooling a new effect external convection cooling (h= 500 W/m^2-K) is added to the reactor model for further analysis. In this model, improved model performance can be described by the following observations: (i) the time required for the model to reach 15°C for the first simulation was measured at 397 seconds, while the second model which incorporated external convection cooling improved upon this time with a value of 195 seconds at a fin aspect ratio of 0.075. (ii) observations of the maximum hotspot temperature within the reactor revealed that the first model generated a high value at 88°C, while the external cooling convection model lowered this reading to 80°C, thereby lowering overall temperatures within the reactor chamber itself. (iii) As can be seen in Figure 4.8 in Section 4.8, there exist two minimum points on the curve which indicate the shortest time needed to reach 15°C, and correspondingly there exist two associated aspect ratios for each value. This is advantageous for physical model assembly and construction due to the fact that the metal hydride reactor can achieve peak cooling performance via two distinct assembly configurations from the standpoint of fin geometry, which in turn gives more flexibility during construction. (iv) Constructal law assists in obtaining the optimal aspect

ratio for fin geometry, and therefore helps to avoid over-complex design which leads to ease of construction and assembly and improved thermal cooling performance.

Nomenclature

c	concentration of the hydrogen, mol m^{-3}
c_p	specific heat, J kg^{-1} K^{-1}
C_a	constant
H_a	activation enthalpy, eV
k	thermal conductivity, W m^{-1} K^{-1}
k_b	Boltzmann constant, eV K^{-1}
κ	permeability, m^2
p_{in}	hydrogen supply pressure, Pa
R	reaction rate, mol m^{-3} s^{-1}

Greek Letters

ε	porosity
μ	viscosity of hydrogen, Pa s
ρ	density, kg m^{-3}

Subscripts

0	initial state
eq	equilibrium
g	hydrogen gas
s	metal hydride powder

4.10 References

1. Leighty, W. Alaska village survival: Affordable energy independence via renewables firmed as hydrogen storage in liquid anhydrous ammonia 2. Alaska: Energy Economy, Villages, Legislation. 2009, 1–11.

2. Isherwood, W.; Smith, J. R.; Aceves, S. M.; Berry, G.; Clark, W.; Johnson, R.; Das, D.; Goering, D.; Seifert, R. Remote power systems with advanced storage technologies for Alaskan villages. Energy 2000, 25, 1005–1020.

3. Rosen, M. a The prospects for renewable energy through hydrogen energy systems. J. Power Energy Eng. 2015, 3, 373–377.

4. Gahleitner, G. Hydrogen from renewable electricity: An international review of power-to-gas pilot plants for stationary applications. Int. J. Hydrogen Energy 2013, 38, 2039–2061.

5. Dodds, P. E.; Staffell, I.; Hawkes, A. D.; Li, F.; Grünewald, P.; McDowall, W.; Ekins, P. Hydrogen and fuel cell technologies for heating: A review. Int. J. Hydrogen Energy 2015, 40, 2065–2083.

6. Corgnale, C.; Hardy, B. J.; Tamburello, D. a.; Garrison, S. L.; Anton, D. L. Acceptability envelope for metal hydride-based hydrogen storage systems. Int. J. Hydrogen Energy 2012, 37, 2812–2824.

7. Nyamsi, S. N.; Yang, F.; Zhang, Z. An optimization study on the finned tube heat exchanger used in hydride hydrogen storage system - Analytical method and numerical simulation. Int. J. Hydrogen Energy 2012, 37, 16078–16092.

8. Souahlia, a.; Dhaou, H.; Askri, F.; Sofiene, M.; Jemni, a.; Ben Nasrallah, S. Experimental and comparative study of metal hydride hydrogen tanks. Int. J. Hydrogen Energy 2011, 36, 12918–12922.

9. Souahlia, a.; Dhaou, H.; Mellouli, S.; Askri, F.; Jemni, a.; Ben Nasrallah, S. Experimental study of metal hydride-based hydrogen storage tank at constant supply pressure. Int. J. Hydrogen Energy 2014, 39, 7365–7372.

10. Garrison, S. L.; Hardy, B. J.; Gorbounov, M. B.; Tamburello, D. a.; Corgnale, C.; Vanhassel, B. a.; Mosher, D. a.; Anton, D. L. Optimization of internal heat exchangers for hydrogen storage tanks utilizing metal hydrides. Int. J. Hydrogen Energy 2012, 37, 2850–2861.

11. R??nnebro, E. C. E.; Whyatt, G.; Powell, M.; Westman, M.; Zheng, F.; Fang, Z. Z. Metal hydrides for high-temperature power generation. Energies 2015, 8, 8406–8430.

12. McWhorter, S.; O'Malley, K.; Adams, J.; Ordaz, G.; Randolph, K.; Stetson, N. T. Moderate Temperature Dense Phase Hydrogen Storage Materials within the US Department of Energy (DOE) H2 Storage Program: Trends toward Future Development. Crystals 2012, 2, 413–445.

13. Felderhoff, M.; Bogdanović, B. High temperature metal hydrides as heat storage materials for solar and related applications. Int. J. Mol. Sci. 2009, 10, 325–344.

14. Sakintuna, B.; Lamari-Darkrim, F.; Hirscher, M. Metal hydride materials for solid hydrogen storage: A review. Int. J. Hydrogen Energy 2007, 32, 1121–1140.

15. K. Nomura, E. Akiba, S. O. J. Less Common Metals. 1983, 89.

16. P. Muthukumar, M.Maiya, S. M. International journal of hydrogen energy. 2005, 30, 1515–1596.

17. G. Lloyd, K.Kim, A. R. Journal of thermophysics Heat transfer. 1998, 12.

18. M. Ron, E. Bershadsky, Y. J. International Journal of Hydrogen Energy. 1992, 17.

19. Congdon, W. US patent. Metal hydride composition and method of making, Patent NO: US 5443616 A, 1995.

20. Dieterich, M.; Pohlmann, C.; Bürger, I.; Linder, M.; Röntzsch, L. Long-term cycle stability of metal hydride-graphite composites. Int. J. Hydrogen Energy 2015, 0, 6–13.

21. Kim, K. J.; Montoya, B.; Razani, A.; Lee, K.-H. Metal hydride compacts of improved thermal conductivity. Int. J. Hydrogen Energy 2001, 26, 609–613.

22. Klein, H. P.; Groll, M. Heat transfer characteristics of expanded graphite matrices in metal hydride beds. Int. J. Hydrogen Energy 2004, 29, 1503–1511.

23. Zimparov, V. D.; da Silva, a. K.; Bejan, a. Constructal tree-shaped parallel flow heat exchangers. Int. J. Heat Mass Transf. 2006, 49, 4558–4566.

24. Bejan, a.; Lorente, S.; Anderson, R. Constructal Underground Designs for Ground-Coupled Heat Pumps. J. Sol. Energy Eng. 2013, 136, 011019.

25. Zhang, H.; Lorente, S.; Bejan, A. Vascularization with line-to-line trees in counterflow heat exchange. Int. J. Heat Mass Transf. 2009, 52, 4327–4342.

26. Bejan, A.; Marden, J. H. The constructal unification of biological and geophysical design. Phys. Life Rev. 2009, 6, 85–102.

27. Rian, I.; Sassone, M. Tree-inspired dendriforms and fractal-like branching structures in architecture : A brief historical overview. Front. Archit. Res. 2014, 3, 298–323.

28. Hadjistassou, C.; Bejan, a.; Ventikos, Y. Cerebral oxygenation and optimal vascular brain organization. J. R. Soc. Interface 2015, 12, 20150245–20150245.

29. G. Majer, U. Kaess, R. B. J. Physical review B. 1998, 57.

30. Website http://www.comsol.com/ for more information about COMSOL multiphysics. 2015, accessed on 03/01/2016

Chapter 5

5 Conclusions

At length, the preceding has discussed in depth the merits of constructal theory and its application into the research of heat transfer, design, and optimization. Herein, a "flow" represents movement of one entity relative to another, and in order to describe this flow, it must be specified what the flow carries with it, how much it carries, and where its source and destination are located . It can therefore be inferred that a flow system inherently contains within it configuration and design.

In the present research, I am investigating to enhance the thermal/heat transfer performance using constructal law of two different features one is thermosyphon evaporator in permafrost regions, and the other is metal hydride reactor for hydrogen energy storage.

The following are the conclusions drawn from the preceding Chapters.

In the Chapter 2, tree shaped designs are proposed using constructal theory to determine the optimal spacing between the two neighboring thermosyphon evaporators, which are used to stabilize the structures from thawing in the permafrost regions. A volumetric model of a road way embankment is referred from a well-known journal and numerical simulations were performed in COMSOL™ for volume averaged temperature against the existing parallel structure evaporators versus tree shaped designs. For a fair comparison, the volume fraction ratio (φ) is maintained constant for all the design models. The following are the observations drawn from Chapter 2:

a) Thermal performance of the different design architectures are analyzed and compared against each other. The critical parameter in deciding the optimum spacing of the two neighboring thermosyphons is volume averaged temperature, the lower is the value the best is the design. A successful study of the architectures located within a conducting medium for different bifurcation levels was made. From the numerical simulations, it is noticed that there exists an optimal spacing.

b) T-shaped structure in the first bifurcation level yields minimal volume averaged temperature outperforming Y-shaped and parallel designs. The optimal spacing for the first bifurcation resulted in the T shaped structure, which was 5.5 m.

c) Y-shaped structures outperform T-shaped design for bifurcation level 2 for optimal spacing, with 7m.

Coming to the Chapter 3, the same constructal theory was used to find the optimal aspect ratio of the fin, which is used to reject heat released in the exothermic reaction of the metal hydride process in hydrogen absorption. The main aspects of this study are to minimize the hot spot temperature and time elapsed for hydrogen absorption process by determining the number and shape of the rectangular fins. The results are compared with different set of cases, single level six fin design, In Case A; the fins are modeled and analyzed for optimization of two-level 12-fin (6 long and 6 short fins) reactor with the fin thickness ratio of 1:1, and Case B; the fins are modeled with the fin thickness ratio of 2:3. Too long fins (low aspect ratio designs) are ineffective for the hotspot located in the middle of the sliced-pizza area while too short fins (high aspect ratio designs) are vulnerable to hotspots in the center of the circular reactor. There exists an optimum aspect ratio to achieve best thermal performance. The Case B design performs the

best results when compared to other two designs. If design complexity is not a factor to consider, a design with many fins are recommended.

In Chapter 4, constructal theory is adapted to find the optimal aspect ratio of the rectangular fin, in this design there is a center coolant channel (the central tube) in the axial direction. The reactor cylinder employs a series of internally mounted rectangular fins, which act as increased cooling surface area to absorb the heat generated from the exothermic hydriding reaction. The simulation study illustrates that there exists an optimal aspect ratio is derived from the COMSOL simulations. Furthermore, an additional study is done with the external cooling effect, and the finding shows improved level of performance in the process time and hotspot reduction in hydrogen absorption process.

6 Appendix

6.1 Distribution of Permafrost

Permafrost underlies approximately 24% of the global land mass. By far the largest portion occurs in the northern hemisphere, mostly Canada, USSR, and Alaska. The ground surface energy balance may become disturbed by certain factors, and that those cause its internal temperature and surface temperatures to vary, the following factors influence the appearance of permafrost:

1. Climate (air temperature, wind) and this influences surface and air temperatures, where by MAST (Mean Annual Surface Temperature) stays below 0°C.

2. Physical terrain (topology, slope) and regions such as high latitude (polar region), high altitude (mountain region) has continental and maritime climates respectively. Continental is worse than maritime at the same latitude.

3. Hydrology (surface drainage, underground water, flooding etc.)

4. Vegetation, which has the capability to inhibit the influence of solar radiation and air temperature.

5. Geology (Soil and rock properties, geothermal heat flow), thermal properties such as thermal conductivity and heat capacity plays a major role.

6. Geothermal heat flux under the permafrost layer plays a vital role in determining temperature and thickness of the permafrost.

7. Snow cover, which acts as an insulation barrier against the heat loss in winter and the surface warming in the spring.

Area Covered(Km^2 x 10^6)			
	Continuous	Discontinuous	Total
Northern Hemisphere	7.64	14.71	22.35
Antarctica	13.21	-----	13.21
Mountains	-----	2.59	2.59
Totals	20.85	17.30	38.15

6.1.1 Types of Permafrost

From the geographer's point of view, there exist various types of permafrost, for which the four main types are classified as follows:

• Continuous permafrost this is associated with the Arctic and Polar regions, and refers to an atmosphere where 80% of the all ground surface has underlying strata of permafrost.

• Discontinuous permafrost category encompasses those environments where 30~80% of the ground surface has an underlying permafrost layer.

• Sporadic permafrost layer is that which has 30% or less existing under the topsoil surface, which mainly depends on the existence of organic soils which help preserve the layer.

• Isolated permafrost is that category in which there exist practically zero trace amounts of permafrost under the ground layer.
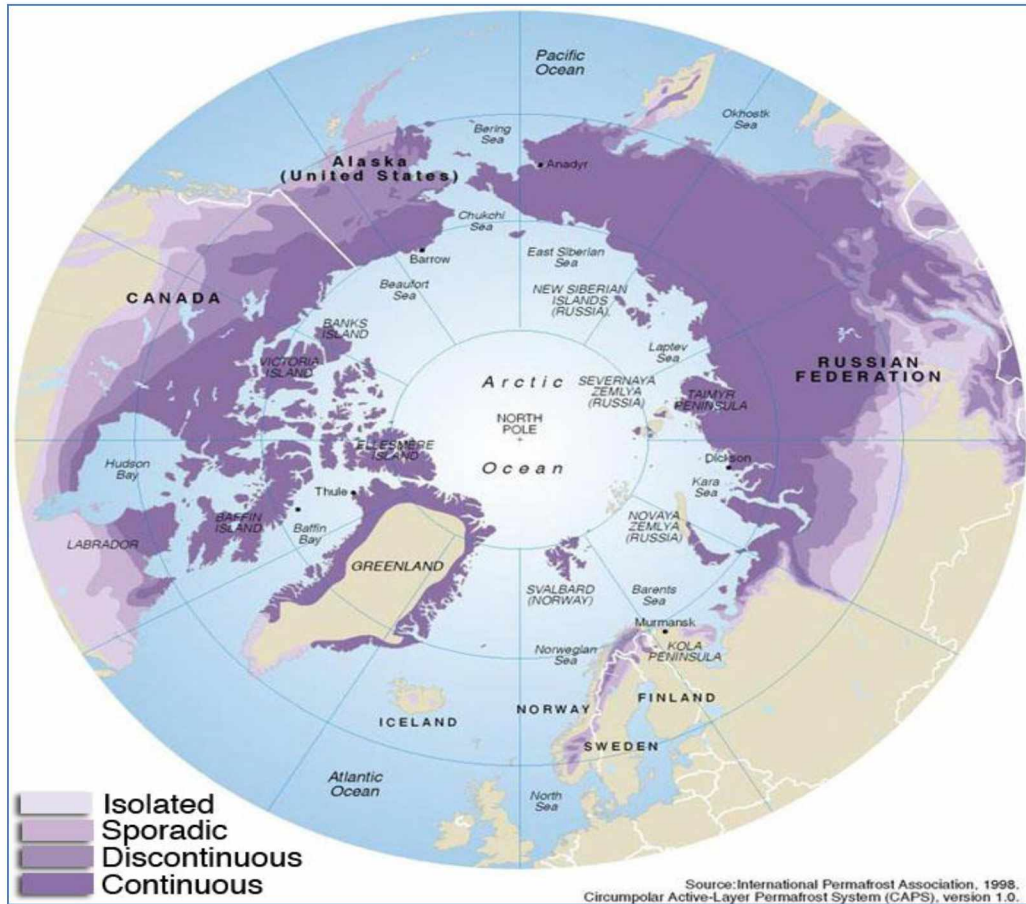
Figure A1: Global permafrost distribution [2]

6.1.2 References

[1] Global Geomorphology by Michael A. Summerfield, Longman Scientific & Technical, 1991

[2] International Permafrost Association, 1998

6.1.3 Journal Publications / Conference Proceedings

[1] Optimum configuration for roadway embankment stabilization on permafrost using constructal law, 3rd International Conference and Exhibition on Mechanical & Aerospace Engineering, October 05-07, 2015 San Francisco, USA

[2] Metal hydride reactor design optimization for hydrogen energy storage, Paper ID: EE011 2016 International Conference on Sustainable and Renewable Energy Engineering, Seoul, South Korea, May 5-7, 2016 (Accepted)

[3] Kukkapalli, K., Kim, SW., 2016, ″Cylindrical Metal hydride reactor design for rapid hydrogen absorption″ (Editorial Review), Energies: ID-126567